Membrane Orientation and Lateral Diffusion of BODIPY-Cholesterol as a Function of Probe Structure

Lukasz M. Solanko,[†] Alf Honigmann,[¶] Henrik Skov Midtiby,[‡§] Frederik W. Lund,[†] Jonathan R. Brewer,[†‡] Vjekoslav Dekaris,[‖] Robert Bittman,[‖] Christian Eggeling,[¶**] and Daniel Wüstner[†*]

[†]Department of Biochemistry and Molecular Biology, [‡]MEMPHYS Center for Biomembrane Physics, Department of Pharmacy, Chemistry and Physics, and [§]Institute for Chemical, Biological and Environmental Technology, University of Southern Denmark, Odense M, Denmark; [¶]Max Planck Institute for Biophysical Chemistry, Department of NanoBiophotonics, Am Fassberg 11, Göttingen, Germany; [‖]Department of Chemistry and Biochemistry, Queens College, The City University of New York, Flushing, New York; and **Human Immunology Unit, Weatherall Institute of Molecular Medicine, University of Oxford, Oxford, United Kingdom

ABSTRACT Cholesterol tagged with the BODIPY fluorophore via the central difluoroboron moiety of the dye (B-Chol) is a promising probe for studying intracellular cholesterol dynamics. We synthesized a new BODIPY-cholesterol probe (B-P-Chol) with the fluorophore attached via one of its pyrrole rings to carbon-24 of cholesterol (B-P-Chol). Using two-photon fluorescence polarimetry in giant unilamellar vesicles and in the plasma membrane (PM) of living intact and actin-disrupted cells, we show that the BODIPY-groups in B-Chol and B-P-Chol are oriented perpendicular and almost parallel to the bilayer normal, respectively. B-Chol is in all three membrane systems much stronger oriented than B-P-Chol. Interestingly, we found that the lateral diffusion in the PM was two times slower for B-Chol than for B-P-Chol, although we found no difference in lateral diffusion in model membranes. Stimulated emission depletion microscopy, performed for the first time, to our knowledge, with fluorescent sterols, revealed that the difference in lateral diffusion of the BODIPY-cholesterol probes was not caused by anomalous subdiffusion, because diffusion of both analogs in the PM was free but not hindered. Our combined measurements show that the position and orientation of the BODIPY moiety in cholesterol analogs have a severe influence on lateral diffusion specifically in the PM of living cells.

INTRODUCTION

Understanding the lateral organization of cholesterol in the plasma membrane (PM) is of major importance for development of new models of cell membrane structure and organization (1). One prominent model assumes lipid-based domain architecture in so-called rafts stabilized by specific sphingolipid-cholesterol interactions. In its original form, that model proposed lateral enrichment of cholesterol in ordered domains in the PM (2). Attempts to visualize sterol domains in the PM using the intrinsically fluorescent close cholesterol mimics cholestatrienol (CTL) and dehydroergosterol (DHE), however, were unsuccessful, and apparent enrichment was found to be a direct consequence of the high submicroscopic curvature of the cell surface (3,4). Characterization of membrane heterogeneity has been performed by several biophysical methods and agreement exists that eventual formation of nanoclusters depends on cholesterol and the cytoskeleton (5–7). How cholesterol itself moves in the PM, however, remains enigmatic. Although intrinsically fluorescent sterols are theoretically the probes of choice to answer this question, the unfavorable photophysical properties of DHE and CTL, which include ultraviolet absorption and ultraviolet fluorescence, low quantum yield, and high photobleaching propensity, make measurement of sterol dynamics within membranes using these cholesterol analogs very challenging. Most cholesterol analogs with an extrinsic fluorophore, however, such as cholesterol tagged with nitrobenzoxadiazole (NBD) fail to behave like cholesterol in model and cell membranes (8,9). Bodipy-cholesterol (B-Chol) (Fig. 1 *A*) is a recently designed cholesterol analog with similar, although not identical, properties to cholesterol and CTL or DHE (10–12). B-Chol partitions into the liquid ordered (l_o) phase in ternary model membranes, although with lower affinity than DHE (12–15). It is transported from the PM to recycling endosomes with similar kinetics and ATP-dependence as DHE, but shows some miss-targeting to lipid droplets in cells with high fat content (12,16). Recently, we demonstrated the potential of B-Chol for tracking vesicular sterol transport with high accuracy, allowing for comparison with diffusion models and for determination of the impact of the cytoskeleton on sterol trafficking (17).

It is well known that cholesterol increases the ordering of phospholipid acyl chains and thereby increases the lateral packing of lipids in the bilayer (18). This property of cholesterol is central for its function in regulating membrane fluidity, bending rigidity, and permeability. The tilt, i.e., the rotation of cholesterol's long molecular axis relative to the bilayer normal has been proposed to be a main determinant of the ability of this sterol to order phospholipid acyl chains and condense lipid bilayers (19). NMR and fluorescence spectroscopy in concert with neutron scattering experiments showed that, despite its strong average orientation, cholesterol undergoes anisotropic motion in the bilayer; fast rotation in discrete jumps is paralleled by rapid out-of-plane diffusion parallel to the membrane normal, both with GHz frequency (20,21). Attachment of fluorophores to cholesterol

Submitted June 26, 2013, and accepted for publication September 16, 2013.

*Correspondence: wuestner@bmb.sdu.dk

Editor: Tobias Baumgart.

0006-3495/13/11/2082/11 $2.00

http://dx.doi.org/10.1016/j.bpj.2013.09.031

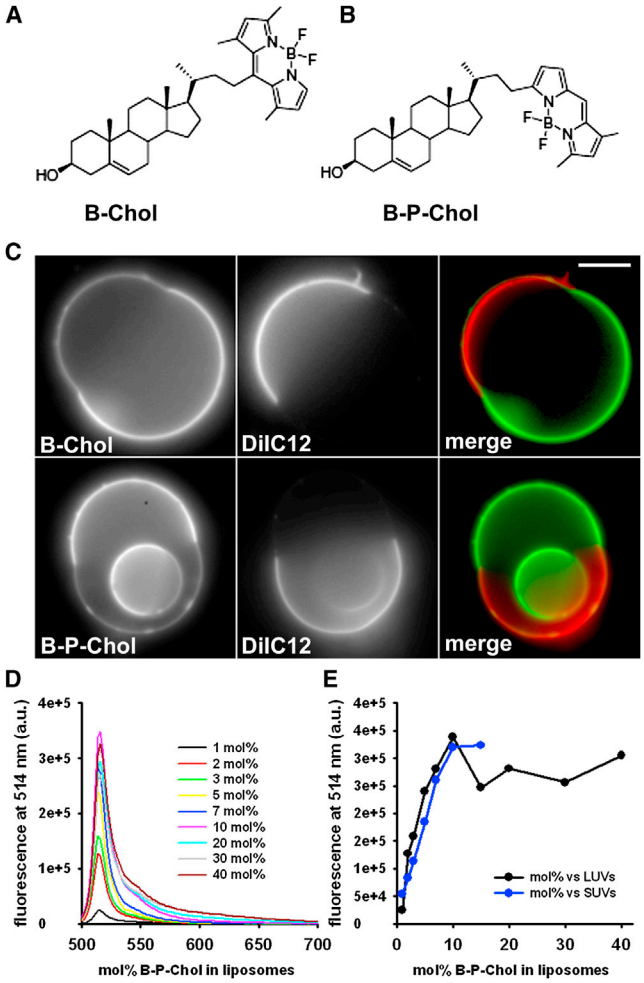

FIGURE 1 Structure, domain partitioning, and self-quenching of BODIPY-cholesterol probes. (*A* and *B*) Structure of B-Chol (*A*) and B-P-Chol (*B*). (*C*) Partitioning of B-Chol (*upper row*) and B-P-Chol in GUVs with l_o/l_d phase coexistence. GUVs were prepared from DPPC, DOPC, and cholesterol in mol percentages of 33:33:33 together with 0.5 mol % of DiIC12 and either B-Chol or B-P-Chol (0.5 mol %) and imaged on a wide field microscope as described in the Supporting Material. Both sterol probes enrich in the DiIC12 poor l_o phase (*green in color* merge in the *most right panels*). (*D*) Emission spectra of B-P-Chol in LUVs made of POPC and increasing concentrations of the sterol probe. A characteristic fluorescence peak at 515 nm but no red-shifted side maximum as in other BODIPY-lipids is found. (*E*) The emission peak at 515 nm was plotted as a function of the probe mole fraction in LUVs (*black symbols* and *line*) and SUVs (*blue symbol* and *line*). Scale bar = 10 μm.

is expected to increase the molecular tilt and thereby locally perturb the membrane structure. This has been observed in molecular dynamics (MD) simulations of B-Chol compared to cholesterol (10). Thus, to assess the potential of fluorescent analogs of cholesterol to mimic the properties of endogenous cholesterol requires taking the orientation of the flurophore into account. Here, we report the synthesis and characterization of a new, to our knowledge, BODIPY-cholesterol analog with a pyrrole-linked BODIPY group to carbon-24 of cholesterol (B-P-Chol) (Fig. 1 *B*). We have assessed several membrane properties of B-P-Chol, including self-quenching propensity and partitioning between l_o and liquid-disordered (l_d) phases in model membranes, and compared them with B-Chol, the classical BODIPY-cholesterol derivative. We demonstrate using two-photon absorption at multiple polarization states that the orientation of the BODIPY-moiety depends on the membrane cholesterol content with larger probe restriction in the presence of cholesterol. Most importantly, we found that under physiological conditions the fluorophore in B-P-Chol is oriented parallel to lipid acyl chains, whereas in B-Chol it is oriented perpendicular to lipid acyl chains. Additionally, the orientation strength was much higher in B-Chol compared to B-P-Chol. The difference in orientation has a strong influence on the lateral diffusion constant of the Chol-analogs in the PM. Using fluorescence recovery after photobleaching (FRAP) and fluorescence correlation spectroscopy (FCS) we found that B-P-Chol diffuses significantly faster than B-Chol in cell membranes. The difference in lateral diffusion is most likely not caused by anomalous subdiffusion processes, as variable spot size FCS measurement on a stimulated emission depletion (STED) microscope (22,23) revealed normal Brownian motion for both probes. Potential reasons for these differences in light of current models of lateral diffusion in lipid membranes are discussed.

MATERIALS AND METHODS

Lipid reagents

BODIPY-cholesterol with the fluorophore attached to the central dipyrrometheneborone difluoride ring (B-Chol) was synthesized as described previously (11). The new Bodipy-cholesterol derivative (denoted here as B-P-Chol; see Fig. 1) in which the fluorophore is linked to C-24 of cholesterol at C-3 of a pyrrole ring of BODIPY was synthesized as described in the Supporting Material. 1-Palmitoyl-2-oleoyl-*sn*-glycero-3-phosphocholine (POPC), 1,2-dipalmitoyl-*sn*-glycero-3-phosphocholine (DPPC), 1,2-dioleoyl-*sn*-glycero-3-phosphocholine (DOPC), and a marker for the liquid-disordered phase, 1,1'-didodecyl-3,3,3′,3′-tetramethylindocarbocyanine perchlorate (DiIC12) were purchased from Avanti Polar Lipids (Alabaster, AL). All other chemicals were from Sigma Chemical (St. Louis, MO).

Measurements

The preparation of small, large, and giant unilamellar vesicles (SUVs, LUVs, and GUVs) as well as of supported bilayers, the culture of baby hamster kidney (BHK) and epithelial kidney (Vero) cells, spectroscopy of B-P-Chol in liposomes, multicolor wide field and two-photon excitation fluorescence microscopy, image analysis for polarization measurement, FRAP, and FCS as well as STED microscopy and its analysis are described in the Supporting Material.

RESULTS

Phase partitioning and fluorescence properties of B-P-Chol

An essential physical characteristic of any suitable fluorescent analog of cholesterol is the ability to partition

into the l_o phase in model membranes made of phospholipids with varying melting temperature. In GUVs one can induce l_o/l_d phase coexistence and find microscopically observable phase separation. Because cholesterol induces formation of the l_o phase, fluorescent sterols with a close resemblance of cholesterol should partition preferentially into the l_o phase. For example, the intrinsically fluorescent sterols, DHE and CTL have been shown to partition into the l_o phase with high preference (12,24). As shown in Fig. 1 *C*, B-P-Chol partitions preferentially into the l_o phase at the expense of the fluid l_d phase. As a marker for the liquid l_d phase, we chose DiIC12, because it localizes exclusively to that phase in GUVs made of DPPC/DOPC/cholesterol (1:1:1) (12). We found a very similar partition preference for B-P-Chol and B-Chol; quantification of BODIPY fluorescence for both probes in GUV images suggests a distribution of both sterols of ~1.5:1 to 2:1 between the l_o and l_d phases. To rule out that fluorophore self-quenching or similar photophysical nonlinearities (e.g., homoenergy transfer) compromise fluorescence measurements, we recorded emission spectra of B-P-Chol at varying concentrations in SUVs and LUVs (Fig. 1 *D*). Peak fluorescence of B-P-Chol at 515 nm was proportional to sterol probe concentration in liposomal membranes up to 10 mol %. Above that concentration, self-quenching of B-P-Chol was found, as inferred from a plateau of the probe's fluorescence emission for increasing mole fraction of the sterol in the bilayer (Fig. 1 *E*). Because we used only 0.5 mol % of the sterols in the partition experiments, self-quenching does not influence these measurements. We previously reported self-quenching of B-Chol in POPC liposomes at >3 mol % (12). Some BODIPY-tagged lipids have been observed to emit red-shifted fluorescence for increasing probe concentration in membranes (25). For example, a characteristic red-shifted emission peak was observed for BODIPY-tagged sphingolipids in bulk spectral measurements and subsequently used to determine probe concentration in model and cellular membranes (26). Interestingly, we did not find a red-shifted emission peak for B-Chol (12) or for B-P-Chol in similar bulk spectral measurements (Fig. 1 *D*). The molecular basis for the differences in emission spectra between various BODIPY-tagged lipids is not known. Similar as here for BODIPY-tagged cholesterol probes, no red-shifted emission could be detected in a recent study for a BODIPY analog of phosphatidylserine (27). In the absorption spectrum of B-Chol, we previously found a characteristic peak at 554 nm above the self-quenching probe concentration (12). This is characteristic for dark ground state dimers (excitons), which efficiently lower the probe fluorescence intensity, because fewer molecules become excited by the incident light. No such absorption peak was found in the spectrum of B-P-Chol (data not shown), suggesting that the quenching mechanisms of B-P-Chol and B-Chol are not identical.

Orientation of B-Chol and B-P-Chol in GUVs studied by polarization microscopy

An important parameter affecting membrane properties and fluorescence characteristics of any lipid probe is the molecular orientation of the attached fluorophore. For example, NBD-tagged phospholipids and sterols show artificially low membrane packing because of back-looping of the NBD moiety to the bilayer-water interface (28). The degree of this interfacial orientation of the NBD moiety was found to depend on the lipid composition and phase state of the bilayer (29). Fluorescence polarization microscopy is a well-known method to determine probe orientation in model and cell membranes. Use of two-photon excitation has several advantages for this purpose, including less scattering, intrinsic sectioning capability with ~300 and ~800 nm lateral and axial resolution, respectively, and, as we showed recently, high photostability of BODIPY-tagged cholesterol, making long-term observation and acquisition of several hundred frames without detectable photobleaching possible (17). For rod-like molecules (such as most laser dyes) the excitation probability is proportional to $\cos^4$ of the angle between the polarization plane of the excitation light and the main transition moment of the fluorophore. This gives a much higher extinction of the fluorophore than that found using single photon excitation, where the excitation probability is proportional to $\cos^2$ (30,31). By rotating the polarization plane of the incident light given by a femtosecond pulsed infrared laser over a full circle, we imaged B-Chol and B-P-Chol in GUVs prepared from POPC by polarized two-photon excitation microscopy (Fig. 2). Clearly, fluorescence of B-Chol follows the orientation of the incident light vector, $\boldsymbol{E}$, and is maximal when the incident light is oriented approximately parallel to the bilayer plane (Fig. 2 *A*; *white arrows* indicate the orientation of the incident light). A plot of fluorescence versus orientation of the incident light for a selected area on the top of the GUVs (*white box* in Fig. 2 *A*) shows two major peaks at ~0^0 and ~180°, respectively, and two minor peaks shifted by 90° relative to the large peaks (Fig. 2 *C*, *blue symbols*). Assuming a $\cos^4$ dependence, we fit the data to a two-component nonlinear cosine function of the form:

$$F(\theta) = A_1 \cdot \cos\left(\theta - \theta_0^1\right)^4 + A_2 \cdot \cos\left(\theta - \theta_0^2\right)^4 + F_0. \quad (1)$$

Here, θ is the rotation angle for the incident linearly polarized light vector, $\boldsymbol{E}$; $A_{1,2}$ are the peak amplitudes of the measured fluorescence and θ_0^1, θ_0^2 describe the orientation of the major fluorophore transition relative to the excitation vector, $\boldsymbol{E}$. The term F_0 describes background fluorescence or detector offset. We found that this function accurately describes the data (Fig. 2 *C*, *blue straight line*), whereas one with only one nonlinear cosine function missed the small peak (Fig. 2 *C*, *blue dashed line*). The dependence of B-P-Chol's fluorescence on the orientation of the incident light

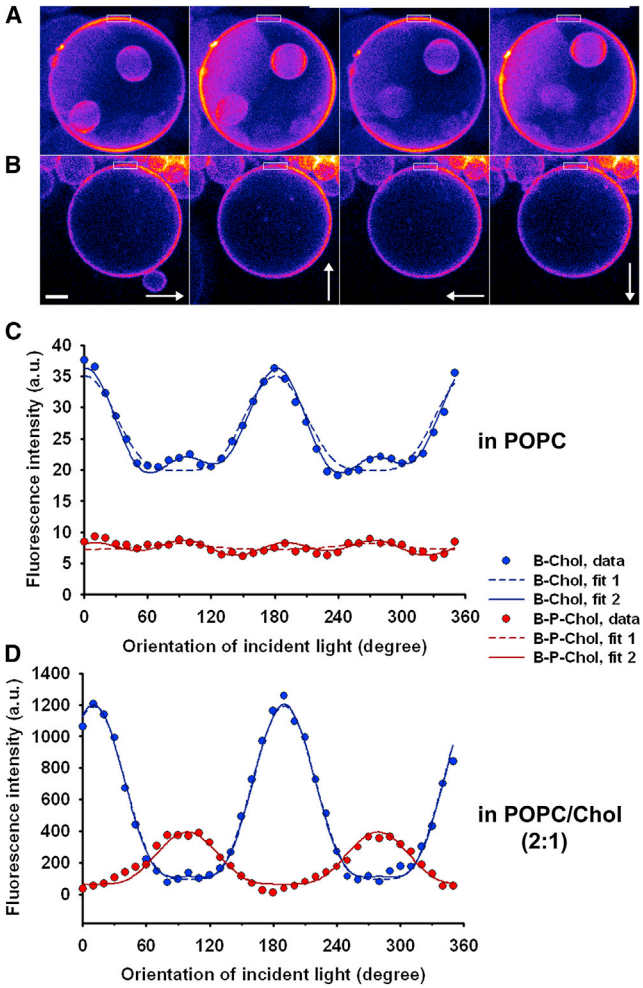

FIGURE 2 Two-photon fluorescence polarimetry of BODIPY orientation in model membranes. GUVs made of POPC and either B-Chol (*A*) or B-P-Chol (*B*) in mol percentages of 99:1 were imaged on a two-photon microscope with 10° rotation of the incident linearly polarized electric field vector, ***E***. The start position of ***E*** is horizontal, as indicated in the most left panel of *B*. Fluorescence intensities of both BODIPY-cholesterol probes were color-coded using a FIRE look-up table with high intensities in yellow/white and low intensities in blue. (*C*) Emission intensities were recorded for the small ROI on top of the GUVs (*rectangular white box* in *panels A*, *B*) for B-Chol (*blue symbols*) and B-P-Chol (*red symbols*) as a function of the orientation of ***E***. The straight blue and red lines show a fit of the data to Eq. 1. The dashed lines show a fit to Eq. 1 with the second amplitude, A_2 set to zero. (*D*) Fluorescence response of B-Chol (*blue symbols* – data, *blue straight line*, fit to Eq. 1 with $A_2 = 0$) and B-P-Chol (*red symbols* – data, *red straight line*, fit to Eq. 1 with $A_2 = 0$) in GUVs made of POPC, cholesterol (80:20 mol percentages). Scale bar = 5 μm.

is much less pronounced (Fig. 2, *B* and *C*, *red symbols*). This can be inferred from the much lower amplitude of fluorescence peaks compared to B-Chol (note that we verified independently, that the same amount of fluorophore was incorporated into both types of GUVs). The data for B-P-Chol were also accurately described by the model shown in Eq. 1 with peaks at the same orientations of incident light as found for B-Chol (i.e., 1.: 0–5°; 2.: ~90°; 3.: 180–190°; 4.: ~270°). However, the first and fourth peaks were much smaller than for B-Chol and of comparable height as the other two peaks. Thus, we found four maxima of fluorescence for comparable orientations of incident light for both BODIPY-tagged cholesterols in GUVs made of only POPC. The major difference is the fluorescence amplitude, which is large only for B-Chol's first and third fluorescence peak (i.e., at ~0^0 and ~180°). We can conclude that B-Chol gets preferentially excited when the incident light vector, ***E***, is parallel to the major transition axis in the BODIPY-moiety in B-Chol lying almost parallel to the bilayer normal in POPC membranes.

When cholesterol is added to a fluid membrane, the phospholipid acyl chains become ordered and more tightly packed. To test this influence on our fluorescent sterol probes, we performed the same measurements in POPC liposomes containing 30 mol % cholesterol. We observed a strong increase in the fluorescence amplitudes of the first and third peak for B-Chol (i.e., at ~0^0 and ~180°), although the second and fourth peak disappeared (Fig. 2 *D*, *blue symbols*). Fitting this data to the model in Eq. 1 revealed that one cosine^4 component is sufficient to describe the data, whereas adding the second term did not yield any improvement in fit quality (Fig. 2 *D*, *dashed* and *straight blue line*, lying on top of each other). From that fit, one can retrieve a mean orientation value but no information about the orientation strength of the fluorescent moieties. The latter can be inferred from a modified equation, where the fluorophore orientation is assumed to be normal distributed around its mean value θ^0 with a standard deviation σ. For two-photon excitation and one dominant probe orientation this gives the following expression for the fluorescence response (with the same notation as above, see the Supporting Material for derivation):

$$F(\theta) = \frac{3 \cdot A_1}{8} + \frac{A_1}{2} \cdot \cos\left(2\theta - 2\theta_0^1\right) \cdot \exp\left(-2\sigma^2\right) + \frac{A_1}{8} \cdot \cos\left(4\theta - 4\theta_0^1\right) \cdot \exp\left(-8\sigma^2\right) + F_0. \quad (2)$$

Fitting this function to the data of both BODIPY-tagged cholesterols in GUVs made of POPC/cholesterol gave a mean orientation of $\theta^0 = 10 \pm 0.08\ ^0$ and $\theta^0 = 98.8 \pm 0.3\ ^0$ relative to the incident field (i.e., perpendicular to the bilayer normal, see *arrows* in Fig. 2) for B-Chol and B-P-Chol, respectively (Fig. S1). The larger angle variation for B-P-Chol reflects the fact that the orientation strength of this cholesterol analog is significantly lower compared to B-Chol.

In two-photon excitation the transition moment is not a 3-component vector (as found for the one-photon case) but a 3 × 3 absorption tensor, because two absorption events have to take place simultaneously. The shape of this tensor is determined by the molecular geometry and sets the limits of observable polarized absorption. If this tensor is highly

asymmetric with only xx-elements being nonzero (defined by Cartesian indices along the molecule long axis), the photoselection is more pronounced than in one-photon excitation and follows a $\cos^4$-law. This is strictly speaking only found in rod-like molecules, such as linear polyenes, where each of the two photons uses a transition moment in the same direction (30,32). The BODIPY moiety belongs to the C_2 molecular symmetry group and therefore has two perpendicular orientations of preferred absorption (33). We found, however, only one dominating orientation in membranes condensed by adding cholesterol, and the $\cos^4$-function was able to fit the fluorescence response exactly (Fig. 2 *D*). For that reason and the sake of simplicity of the mathematical treatment of the data, we assumed only one transition moment in our analysis, as suggested previously for the BODIPY fluorophore (32) as well as for other not strictly rod-like probe molecules (34).

Orientation of B-Chol and B-P-Chol in cell membranes

We explored the photoselection effect further to determine the orientation of the BODIPY fluorophore attached to cholesterol in the PM of BHK cells. By rotating the electric field vector of the incident light around an axis perpendicular to the image (*xy*-) plane, we found that emission of B-Chol in plane membrane regions exactly followed the rotating excitation field. Due to the complex topography of cellular membranes, we have implemented a pixel-based analysis of the fluorescence response for this data (for details of that method, see the Supporting Material and (35)). Briefly, the orientation-dependent fluorescence is decomposed into Fourier components, and two ways of expressing the extracted physical parameters were used in images of GUVs (Fig. S2) and of cells (Fig. 3, Fig. S3 and Fig. S5). In the color-coded representation, the phase of the fluorescence response relative to the rotating incident vector is translated into probe orientation and expressed in the hue, saturation, and value color model (Fig. 3, *A* and *C*; see Fig. S2 *C* for the *color legend*). In the vector-coded representation, the amplitude (i.e., orientation strength) and phase (i.e., orientation angle) of the probe relative to the incident light vector are given as length and direction of small blue lines in each pixel position (e.g., in Fig. 3, *B* and *D*). Using this analysis, we found that the BODIPY group is oriented perpendicular to the bilayer normal for B-Chol in straight regions of the PM of living BHK cells (Fig. 3, *A* and *B*, and Fig. S3). In contrast, in regions with high surface ruffling, as on cell edges and surface protrusions, the fluorescence response to the rotating excitation vector was low. To determine whether this is a consequence of the local surface curvature or caused by a second population of nonoriented B-Chol molecules, we studied the fluorescence response in cells with disrupted actin cytoskeleton (Fig. 3, *C* and *D*). Treatment of cells for 30 min with 20 μM cytochalasin D induced formation of membrane blebs (3),

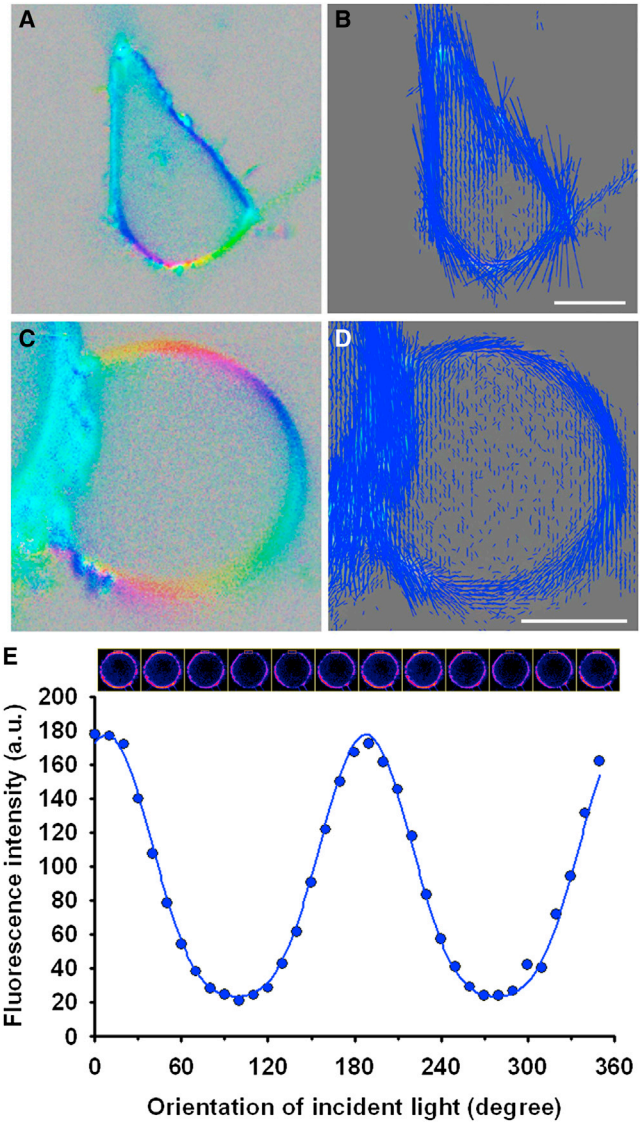

FIGURE 3 Two-photon fluorescence polarimetry of B-Chol in the PM of BHK cells. BHK cells were labeled with B-Chol from a B-Chol-CD complex as described in the Supporting Material. Cells were imaged on a two-photon microscope with 10° rotation of the incident linearly polarized electric field vector, ***E***. The start position of ***E*** is horizontal, as indicated in the legend to Fig. 2 *B*. (*A* and *B*) Show the color-coded (*A*) and vector-coded (*B*) presentation of the fluorescence response for intact cells. For *C* and *D*, cells were treated with 20 μM cytochalasin D for 30 min to disrupt the actin and induce bleb formation. The color-coded (*C*) and vector-coded (*D*) presentation of the fluorescence response is shown for a representative bleb. (*E*) Emission intensities were recorded for the small ROI on top of another cytochalasin-treated cell labeled with B-Chol (*blue symbols*) as a function of the orientation of ***E***. The straight blue line shows a fit of the data to Eq. 2. Scale bar = 5 μm.

and we found that the fluorescence response of B-Chol in these blebs is comparable to that in GUVs made of POPC/cholesterol (compare Fig. S2 *A* and Fig. 3, *C* and *D*). Extracting the intensity of B-Chol emission as a function of the orientation of the incident field for a representative cytochalasin-treated cell and fitting the fluorescence

response to Eq. 2 gave a mean orientation of $\theta^0 = 6.21 \pm 0.221\ ^0$ (Fig. 3 *E*). From this result it can be concluded that the angle and strength of the orientation of the BODIPY moiety in B-Chol in cell membranes is comparable to that determined for GUVs containing 30 mol % cholesterol with a strongly confined, almost perpendicular orientation of the flurophore relative to the bilayer normal. In highly convoluted surface regions the orientation of the BODIPY flurophore attached to cholesterol's side chain seems to have no preferred direction but follows the rough surface topography, as also confirmed in measurements of the same cell at varying focus positions (see Fig. S3). Accordingly, in ruffles there is no preferred direction in which the incident excitation light can excite B-Chol, resulting in small, randomly oriented molecular directors **c**. By two-photon time-lapse microscopy, we observed that surface ruffles containing B-Chol are dynamic entities constantly protruding and retracting, thereby changing the local surface topology on a timescale of several minutes (see Fig. S4). When doing the same polarization measurements with B-P-Chol, we found a very low fluorescence response to the rotating incident excitation vector as concluded from the vector- and color-coded representation (Fig. S5). There was a slight tendency toward an orientation of the BODIPY-group of B-P-Chol parallel to the membrane normal, especially after actin disruption (compare Fig. S5 *A*, *B* and *C*, *D*). This result is again largely in agreement with the data of B-P-Chol orientation in GUVs prepared from POPC/cholesterol. It suggests some alignment of the fluorophore in B-P-Chol with the direction of the fatty acyl chains (compare Fig. S2 and Fig. S5). We conclude that the fluorescent moiety in B-P-Chol experiences much less structural confinement in model and cell membranes than the BODIPY group in B-Chol.

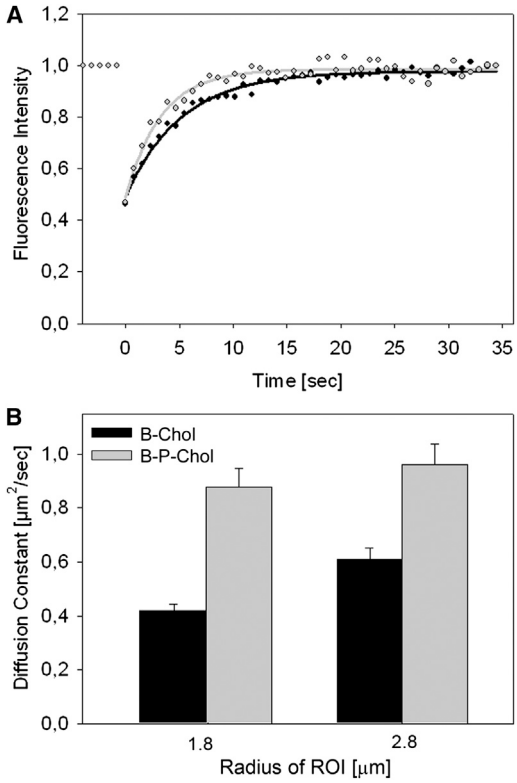

FIGURE 4 FRAP measurement of B-Chol and B-P-Chol in the PM of BHK-cells. FRAP experiments were performed on a Zeiss LSM510 confocal microscope in living BHK cells, as described in the Supporting Material. (*A*) Fluorescence recovery curves for FRAP in a circular ROI with radius $r = 2.8\ \mu$m for both BODIPY-cholesterol analogs. Black and gray symbols show the mean of five measurements for B-Chol and B-P-Chol, respectively. The black and gray lines show the fit of Eq. S2 for B-Chol and B-P-Chol, respectively. (*B*) The FRAP experiment was performed for circular ROIs with radii of 1.8 and 2.8 μm. The bar plot shows the diffusion constants for the B-Chol (*black*) and B-P-Chol (*gray*) for each experiment with error bars of $\pm$ one standard error.

Diffusion of B-Chol and B-P-Chol in model and cell membranes measured by FRAP and FCS

To test whether the angle and strength of fluorophore orientation in the two BODIPY-tagged cholesterol probes affect their lateral diffusion, we first performed FRAP measurements in the PM of BHK cells labeled with either B-Chol or B-P-Chol (Fig. 4). In the FRAP experiment a region of interest (ROI) in the PM is bleached and the fluorescence recovery is imaged over time. For a detailed FRAP protocol see the Supporting Material. Fig. 4 *A* shows the mean of five fluorescence recovery curves for a circular ROI with radius 2.8 μm and the fits of Eq. S2 in blue and red for B-Chol and B-P-Chol, respectively. If the diffusing probes are not trapped in microscopic domains of the PM, the size of the bleached area should not affect the diffusion constant (36,37). To test this, we performed FRAP experiments with ROIs with radii of 1.8 and 2.8 μm, respectively. As shown in Fig. 4 *B*, the size of the bleach ROI had no effect on the measured diffusion constants, whereas B-P-Chol diffused almost twice as fast as B-Chol, i.e., $D_{B\text{-}P\text{-}Chol} = 0.8\text{–}1.0\ \mu m^2/s$ compared to $D_{B\text{-}Chol} = 0.5\ \mu m^2/s$. BODIPY-tagged cholesterol including B-Chol has been shown to move by vesicular and nonvesicular transport between PM and intracellular compartments (12,17). During the laser-based bleaching in a FRAP experiment on a confocal microscope significant photodestruction takes place above and below the focal plane (38). For example, we have recently shown in experiments on fixed cells and in three-dimensional reaction-diffusion simulations that a 63× objective with NA = 1.4 as used here causes photobleaching in a cone shape up to several micrometers beyond the depth of field (see Fig. S2 and S3 in (39)). Because B-Chol diffuses rather slowly in the cytoplasm of mammalian cells (17), it could become necessary to include a cytoplasmic diffusion term into the FRAP analysis. To do so, we have applied the extended FRAP model developed by Berkovich et al. (40) and found an almost identical goodness of fit as with the simple FRAP model (not shown). However,

the estimated parameters including diffusion constants in the PM and cytoplasm and the on-/off-rates between both compartments were associated with a large uncertainty, which led us to conclude that the simple FRAP model given in Eq. S2 is sufficient to accurately describe movement of BODIPY-tagged cholesterol probes in the PM of BHK cells.

To determine the lateral mobility of both BODIPY-tagged cholesterol probes in lipid membranes in more detail, we used FCS. FCS measures the mean transit time of single molecules diffusing through a confocal observation volume. The lateral diffusion constant of the probe can be calculated with high statistical precision by FCS when the size of the confocal volume is known. To determine if the different molecular orientations of B-Chol and B-P-Chol are reflected in the lateral diffusion of both sterol probes, we conducted FCS measurements in model membranes and in live cell membranes (Fig. 5 *A*). We obtained a lateral diffusion constant of D = 3.2 $\mu m^2/s$ for both probes in cholesterol free supported DOPC membranes. In supported membranes made of POPC and 30 mol % cholesterol the lateral diffusion of both cholesterol probes was reduced by a factor of 1.9 to D = 1.7 $\mu m^2/s$. Again, as for the cholesterol-free membranes, we found no significant difference in lateral mobility between the two sterol probes. Finally, we incorporated B-Chol and B-P-Chol in the PM of cultured Vero epithelial kidney cells and determined the lateral diffusion constant with FCS. In agreement with the FRAP experiments in BHK-cells, we found that B-P-Chol diffused significantly faster with $D_{B\text{-}P\text{-}Chol} = 2.6\ \mu m^2/s$ compared to B-Chol, which diffused with $D_{B\text{-}Chol} = 1.7\ \mu m^2/s$. Although the difference in diffusion constants $D_{B\text{-}P\text{-}Chol}/D_{B\text{-}P\text{-}Chol} \approx 1.6$ was roughly the same in BHK and Vero cells, the absolute values differed by a factor of ~3–3.5. This is not surprising, because the absolute diffusion constants can vary between different cell types (5). Even though we performed FCS measurement as soon as possible after staining the PM (2–5 min), we observed that a fraction of the probes had already entered the cytosol of the cells. To exclude the possibility that the difference in lateral diffusion of the two cholesterol analogs was caused by a different partitioning into the cytoplasm or organelle membranes, we produced PM sheets removing the cytosol and inner membranes. In membrane sheets the difference in lateral diffusion of the two cholesterol analogs was in the same range as measured in the PM of intact living cells (see Fig. S6). This supports the conclusion that B-P-Chol indeed moves significantly faster in the PM compared to B-Chol and rules out that a cytoplasmic component of sterol diffusion contributes to the measured differences in PM diffusion.

Probing anomalies in lateral diffusion of B-Chol and B-P-Chol in cell membranes with STED-FCS

To test whether the observed difference between the lateral diffusion of B-Chol and B-P-Chol in the PM (FRAP and confocal FCS) was caused by anomalous subdiffusion processes, for example due to transient trapping of the sterols in subregions of the PM, we applied superresolution STED-FCS (22,23,41). Applying FCS on a STED microscope allows determination of the values of the apparent diffusion coefficient D for different observation spot sizes (tuned for example by the intensity of the STED laser) below the diffraction limit of ~200 nm of conventional optical microscopy (5,23,41). The dependency of D on the diameter d of the observation spots indicates whether diffusion is hindered or not (5,41,42). Constant values of $D(d)$ demonstrate free Brownian diffusion, although a decrease of D toward smaller observation sizes shows hindered diffusion, for example, due to transient interactions with relatively slow moving or immobilized molecules (trapping) (5,43). In our measurements we used a continuous-wave 577 nm STED laser. We set the power of the STED laser to 80 mW and varied the size of the observation spot by gated STED-FCS. In gated STED-FCS, the combination of pulsed excitation and gated detection realizes a reduction of the diameter d of the effective observation spot with increasing temporal shift of the detection window (time gate) with respect to the excitation pulse (44). We first checked whether gated STED-FCS is applicable to the Bodipy-cholesterol probes. To this end, we determined the average transit time of both, B-Chol and B-P-Chol, diffusing in supported lipid bilayers made of POPC + 30 mol % cholesterol for different time gates (Fig. 5 *C*). We could clearly observe a reduction of the transit time with gating position, allowing us to calibrate the dependency of the effective diameter d of the observation spot on the time gate, which was the same for both B-Chol and B-P-Chol. Next, we determined the dependency $D(d)$ for both cholesterol analogs in the PM of Vero cells from diffraction-limited $d = 190$ nm down to $d = 80$ nm (Fig. 5 *E*). Interestingly, the dependency $D(d)$ was almost constant for both analogs, indicating close to free diffusion with only weak transient interactions (or trapping). Accordingly, the difference in lateral diffusion between the probes remained constant when the observation area was decreased, with B-P-Chol diffusing 1.7-fold faster than B-Chol. Furthermore, as shown in Fig. 5 *C*, the extrapolated intercept of the mean transit time for focal areas $\rightarrow 0\ \mu m$ was close to zero for B-Chol and B-P-Chol in accordance with free diffusion of both Bodipy-cholesterol probes (42). Thus, the STED-FCS results show that the difference in lateral diffusion between B-P-Chol and B-Chol is not caused by anomalous subdiffusion processes due to transient molecular interactions.

DISCUSSION

In this study, we introduced a BODIPY-tagged cholesterol analog with the dye being attached to the cholesterol side chain via one of BODIPY's pyrrole rings (B-P-Chol,

Fig. 1 *B*). We demonstrated by two-photon fluorescence polarimetry that the fluorophore in B-P-Chol had a tendency to be aligned along the fatty acyl chains in both, cholesterol containing model membranes and in cell membranes (compare Fig. 2 *B* and Figs. S4, S5). In contrast, B-Chol, the classical BODIPY-tagged cholesterol in which the fluorophore is attached via the *meso*-carbon of the dipyrromethene moiety to cholesterol's side chain, was found to orient its fluorescent group perpendicular to the fatty acyl chains with a much stronger confinement than B-P-Chol in both model and cell membranes (compare Figs. 2 and 3 with Fig. S2 and Fig. S3). The difference in orientation of both probes was not found in cholesterol-free model membranes (see Fig. 2), where B-P-Chol and B-Chol showed a bimodal distribution, as previously reported for other BODIPY-tagged lipid probes (45,46). Interestingly, recent MD simulations also found a perpendicular orientation of the BODIPY moiety of B-Chol in DPPC bilayers with an additional small population of back-looped fluorophores oriented almost parallel to the membrane normal (10). Time-resolved anisotropy measurements of B-Chol in GUVs have confirmed an orientation of the BODIPY group perpendicular to the membrane normal (13). Additionally, the fluorescence anisotropy of B-Chol showed a multiexponential decay pattern in these measurements, which was likely due to several rotational modes of the sterol probe in the bilayer (13). B-Chol distends its fluorophore toward the center of the bilayer, as shown by quenching experiments with spin labels as well as by ^{2}H-NOESY NMR experiments (47). Interestingly, despite its preferred partition into the cholesterol-induced l_o phase (see Fig. 1, *C* and *D*, and (12–15)), B-Chol did not induce acyl-chain ordering in liposomes in a comparable manner to cholesterol (47). The attached BODIPY moiety will likely slow down the rotation of cholesterol's alkyl chain from a mean correlation time of <1 ns (48) to at least 5 ns (13). This will clearly affect some of the physico-chemical properties of the linked cholesterol. Based on our two photon polarimetry experiments, we propose that the BODIPY moiety in B-Chol occupies more space perpendicular to the bilayer normal, which is why it is sterically hindered in its movement and thereby more confined than that of B-P-Chol. A larger free volume for the BODIPY moiety in B-P-Chol is suggested by the lower fluorescence response in the two-photon polarimetry measurements and by the higher onset of fluorophore self-quenching in liposomes for B-P-Chol (i.e., 10 mol %, Fig. 1, *D* and *E*), than for B-Chol (i.e., 3 mol % (12)). One can therefore speculate that the sterol orientation in B-P-Chol is less disturbed by the attached fluorophore than in B-Chol. Consequently, the sterol might be less tilted favoring a more cholesterol-like behavior for B-P-Chol than for B-Chol. Surprisingly, the high protein density in the PM did not change the relative orientation of the BODIPY group in the cholesterol analogs compared to protein free model membranes. This, however, does not exclude the possibility that the rotational dynamics of the BODIPY moiety is different in the protein containing PM compared to model membranes for both cholesterol probes, something which might be explored in future systematic studies (13,47).

The different orientation of the BODIPY-fluorophore did not affect the lateral diffusion of both sterol analogs in model membranes. In supported model membranes made of POPC and 30 mol % cholesterol, the lateral diffusion of both cholesterol probes measured by FCS was comparable and reduced by almost twofold compared to membranes made of DOPC without cholesterol (see Fig. 5 *A*). For B-Chol, this is in line with earlier FCS measurements on GUVs showing that the analog diffuses significantly slower in the cholesterol-rich l_o phase (i.e., 4.98 $\mu m^2/s$) compared to the cholesterol-poor l_d phase (i.e., 7.23 $\mu m^2/s$) (13). Although the lipid composition of the GUVs differed somehow in the study by Ariola et al. from that used here (i.e., ternary mixtures of DOPC/SM/cholesterol were used in the study by Ariola et al. (13)), the overall faster diffusion of B-Chol in GUVs in that study compared to our experiments with supported bilayers is likely a consequence of the friction induced by the solid support when using supported membranes, as thoroughly studied previously (49). The different orientation of the BODIPY-fluorophore had a profound effect on the motion of both BODIPY-cholesterol probes in the PM of living cells. Using FRAP and FCS in two different cell types (Vero and BHK cells), we found a 1.5- to 1.8-fold slower diffusion for B-P-Chol compared to B-Chol (see Figs. 4 and 5). Furthermore, STED-FCS measurements confirmed the results obtained by FRAP and FCS and showed that lateral diffusion of B-Chol and B-P-Chol was not hindered in the PM (see Fig. 5, *C* and *D*, and Fig. S6). The observed relatively free diffusion of the cholesterol analogs is surprising, because cholesterol is supposed to be highly interactive in the PM of living cells, facilitating various molecular interactions (2,5,41). Either the fluorescent BODIPY-tagged analogs, in contrast to their endogenous counterparts, were not involved in such complexes or the transient interactions of cholesterol are weak and characterized by large off-rates compared to on-rates resulting in almost constant $D(d)$ dependencies, as previously determined for fluorescent phosphoethanolamine lipids using STED-FCS (5,41). In fact, it has been shown in simulations, that equilibration of a diffusing species between a finite hierarchy of binders will result in normal diffusion at all timescales (43). However, given that both sterol probes diffuse freely in the PM of living cells, why is there a difference in diffusion constants? In general, lateral diffusion of lipids and small hydrophobic molecules in membranes has been described in the framework of the free volume theory first proposed by Cohen and Turnbull (50), later extended by Macedo and Litovitz by taking Eyrings transition state theory into account (51) and applied in the context of lipid membranes by Almeida,

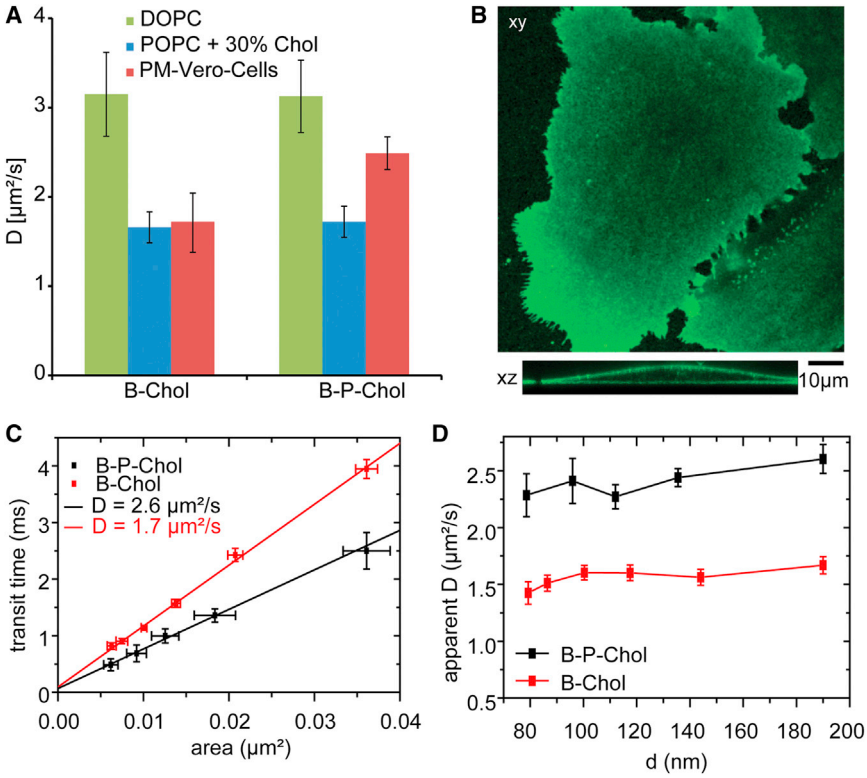

FIGURE 5 FCS and STED-FCS of B-Chol and B-P-Chol in model and cell membranes. (*A*) Diffusion coefficients *D* of B-Chol and B-P-Chol in supported lipid bilayers (DOPC: one-component DOPC; POPC + 30% Chol: two-component system POPC and 30 mol% cholesterol) and in the PM of living Vero cells (PM-Vero-Cells) as determined by (*confocal*) FCS. (*B*) Confocal fluorescence scanning image of a Vero cell labeled with B-P-Chol (*upper panel*: *xy* scan; *lower panel*: *xz* scan). (*C* and *D*) STED-FCS data of B-Chol (*red*) and B-P-Chol (*black*) diffusion in the PM of living Vero cells: average transit time through the observation spot (*C*) and apparent diffusion coefficient *D* (*D*) determined from FCS measurements at different sizes of the observation spot (*C*, area and *D*, diameter *d*). A linear transit-time (*area*) dependency and constant *D*(*d*) values reveal almost free diffusion of both probes with absolute value of *D* indicated in the panels.

Vaz, and co-workers (52). Using FCS, the dependence of lateral diffusion coefficients of fluorescent lipid probes on the mean molecular area has been verified in phospholipid monolayers even in quantitative agreement with the free volume theory (53). The basic idea of the free volume model is that diffusing probes can only step forward from their initial position (i.e., hop), if i), sufficient free volume in the bilayer is transiently generated by thermally or otherwise driven local density fluctuations and ii), the diffusing molecule acquires enough energy to break away its immediate neighbors (54). Because both BODIPY-tagged sterols move freely in the PM, we assume that the second condition is fulfilled for B-Chol and B-P-Chol. Recent extensions of this model suggested by MD simulations take the highly heterogeneous lateral pressure profile in membranes into account (55,56). These simulations show that the free volume is not isotropically distributed but appears transiently in the form of ellipsoidal voids mostly oriented along the fatty acyl chains in a cholesterol-dependent manner (55,56). Membrane-embedded proteins have been found to further lower the free volume and to compress the immediately surrounding bilayer and thereby to lower the diffusion rates of membrane lipids (57,58). Proteins with hydrophobic residues exceeding the bilayer thickness can often deform the bilayer such that it gets locally thicker with a coherence length of 1.5–2 nm (59). Lipids with longer hydrophobic tails tend to cluster around such proteins without binding to them, although at the same time their acyl chains order underneath the headgroup and disorder close to the bilayer center (59,60). In addition, extended MD simulations suggest that these annulus lipids correlate their lateral movement with that of the embedded protein and therefore diffuse much slower than lipids further apart (60,61). In light of these results, we speculate that B-Chol due to its BODIPY-moiety stretching into the bilayer center is more anchored and slightly longer than B-P-Chol. This causes a higher tendency of B-Chol to occupy places adjacent to proteins to avoid its hydrophobic mismatch but also to account for its lower mobility parallel to the bilayer normal (21). As a consequence, B-Chol comes to diffuse more frequently in concert with the much larger membrane-embedded proteins resulting on average in the measured lower diffusion constant compared to B-P-Chol in the PM. Further studies involving NMR and fluorescence spectroscopy as well as simulations of membrane proteins in the presence of the fluorescent sterols might be useful to explore this possibility further. Alternatively, it is possible that B-Chol and B-P-Chol have a different preference for the outer versus inner leaflet of the PM. The cytoplasmic leaflet is rich in the aminophospholipids, phosphatidylserine and phosphatidylethanolamine. The inner leaflet is generally considered as being more fluid than the outer leaflet; the latter being more enriched in sphingolipids with saturated acyl chains (62). Accordingly, the outer leaflet is likely more packed and lateral diffusion of lipids including sterols should be faster in the inner leaflet of the PM. Both predictions have been confirmed in model membrane systems mimicking the outer and inner leaflet lipid composition,

respectively (63–65). Interestingly, the intrinsically fluorescent close cholesterol mimics DHE and CTL have been found to reside mostly in the cytoplasmic leaflet of the PM in fibroblasts and macrophages (66–68). By assuming that B-P-Chol is more enriched in the inner leaflet of the PM than B-Chol, one can easily explain its faster diffusion in the PM and PM sheets compared to B-Chol. Different transbilayer distribution of both BODIPY-cholesterol analogs could even explain why B-P-Chol diffuses faster in the PM than in model membranes containing cholesterol (see Fig. 5 *A*). Future studies in our lab will focus on determining the transbilayer distribution and mobility of B-Chol and B-P-Chol in living cells.

SUPPORTING MATERIAL

Seven figures, twelve equations, six schemes, references (69–72) and supplementary data are available at http://www.biophysj.org/biophysj/supplemental/S0006-3495(13)01079-5.

D.W. acknowledges funding from the Lundbeck, Villum and NovoNordisk foundations, C.E. and A.H. from the Deutsche Forschungsgemeinschaft (DFG) via the SFB937.A.H. and C.E. acknowledge continuous support by Prof. Stefan Hell. The Danish Molecular Biomedical Imaging Center (DaMBIC) and its director Prof. Luis Bagatolli are acknowledged for making the two-photon microscope available.

REFERENCES

1. Munro, S. 2003. Lipid rafts: elusive or illusive? *Cell.* 115:377–388.
2. Simons, K., and E. Ikonen. 1997. Functional rafts in cell membranes. *Nature*. 387:569–572.
3. Wüstner, D. 2007. Plasma membrane sterol distribution resembles the surface topography of living cells. *Mol. Biol. Cell.* 18:211–228.
4. Wüstner, D., and N. J. Faergeman. 2008. Spatiotemporal analysis of endocytosis and membrane distribution of fluorescent sterols in living cells. *Histochem. Cell Biol.* 130:891–908.
5. Mueller, V., C. Ringemann, …, C. Eggeling. 2011. STED nanoscopy reveals molecular details of cholesterol- and cytoskeleton-modulated lipid interactions in living cells. *Biophys. J.* 101:1651–1660.
6. Jaqaman, K., H. Kuwata, …, S. Grinstein. 2011. Cytoskeletal control of CD36 diffusion promotes its receptor and signaling function. *Cell.* 146:593–606.
7. Gowrishankar, K., S. Ghosh, …, M. Rao. 2012. Active remodeling of cortical actin regulates spatiotemporal organization of cell surface molecules. *Cell.* 149:1353–1367.
8. Scheidt, H. A., P. Müller, …, D. Huster. 2003. The potential of fluorescent and spin-labeled steroid analogs to mimic natural cholesterol. *J. Biol. Chem.* 278:45563–45569.
9. Mukherjee, S., X. Zha, …, F. R. Maxfield. 1998. Cholesterol distribution in living cells: fluorescence imaging using dehydroergosterol as a fluorescent cholesterol analog. *Biophys. J.* 75:1915–1925.
10. Hölttä-Vuori, M., R. L. Uronen, …, E. Ikonen. 2008. BODIPY-cholesterol: a new tool to visualize sterol trafficking in living cells and organisms. *Traffic.* 9:1839–1849.
11. Li, Z., E. Mintzer, and R. Bittman. 2006. First synthesis of free cholesterol-BODIPY conjugates. *J. Org. Chem.* 71:1718–1721.
12. Wüstner, D., L. M. Solanko, …, A. Herrmann. 2011. Quantitative assessment of sterol traffic in living cells by dual labeling with dehydroergosterol and BODIPY-cholesterol. *Chem. Phys. Lipids.* 164:221–235.
13. Ariola, F. S., Z. Li, …, A. A. Heikal. 2009. Membrane fluidity and lipid order in ternary giant unilamellar vesicles using a new bodipy-cholesterol derivative. *Biophys. J.* 96:2696–2708.
14. Sezgin, E., I. Levental, …, P. Schwille. 2012. Partitioning, diffusion, and ligand binding of raft lipid analogs in model and cellular plasma membranes. *Biochim. Biophys. Acta.* 1818:1777–1784.
15. Shaw, J. E., R. F. Epand, …, C. M. Yip. 2006. Correlated fluorescence-atomic force microscopy of membrane domains: structure of fluorescence probes determines lipid localization. *Biophys. J.* 90:2170–2178.
16. Jansen, M., Y. Ohsaki, …, E. Ikonen. 2011. Role of ORPs in sterol transport from plasma membrane to ER and lipid droplets in mammalian cells. *Traffic.* 12:218–231.
17. Lund, F. W., M. A. Lomholt, …, D. Wüstner. 2012. Two-photon time-lapse microscopy of BODIPY-cholesterol reveals anomalous sterol diffusion in Chinese hamster ovary cells. *BMC Biophys.* 5:20.
18. Ipsen, J. H., O. G. Mouritsen, and M. Bloom. 1990. Relationships between lipid membrane area, hydrophobic thickness, and acyl-chain orientational order. The effects of cholesterol. *Biophys. J.* 57:405–412.
19. Aittoniemi, J., T. Róg, …, I. Vattulainen. 2006. Tilt: major factor in sterols' ordering capability in membranes. *J. Phys. Chem. B.* 110:25562–25564.
20. Weisz, K., G. Gröbner, …, G. Kothe. 1992. Deuteron nuclear magnetic resonance study of the dynamic organization of phospholipid/cholesterol bilayer membranes: molecular properties and viscoelastic behavior. *Biochemistry.* 31:1100–1112.
21. Gliss, C., O. Randel, …, T. Bayerl. 1999. Anisotropic motion of cholesterol in oriented DPPC bilayers studied by quasielastic neutron scattering: the liquid-ordered phase. *Biophys. J.* 77:331–340.
22. Klar, T. A., S. Jakobs, …, S. W. Hell. 2000. Fluorescence microscopy with diffraction resolution barrier broken by stimulated emission. *Proc. Natl. Acad. Sci. USA*. 97:8206–8210.
23. Kastrup, L., H. Blom, …, S. W. Hell. 2005. Fluorescence fluctuation spectroscopy in subdiffraction focal volumes. *Phys. Rev. Lett.* 94:178104.
24. Baumgart, T., G. Hunt, …, G. W. Feigenson. 2007. Fluorescence probe partitioning between Lo/Ld phases in lipid membranes. *Biochim. Biophys. Acta.* 1768:2182–2194.
25. Marks, D. L., R. Bittman, and R. E. Pagano. 2008. Use of Bodipy-labeled sphingolipid and cholesterol analogs to examine membrane microdomains in cells. *Histochem. Cell Biol.* 130:819–832.
26. Chen, C. S., O. C. Martin, and R. E. Pagano. 1997. Changes in the spectral properties of a plasma membrane lipid analog during the first seconds of endocytosis in living cells. *Biophys. J.* 72:37–50.
27. Kay, J. G., M. Koivusalo, …, S. Grinstein. 2012. Phosphatidylserine dynamics in cellular membranes. *Mol. Biol. Cell.* 23:2198–2212.
28. Chattopadhyay, A., and E. London. 1987. Parallax method for direct measurement of membrane penetration depth utilizing fluorescence quenching by spin-labeled phospholipids. *Biochemistry.* 26:39–45.
29. Raghuraman, H., S. Shrivastava, and A. Chattopadhyay. 2007. Monitoring the looping up of acyl chain labeled NBD lipids in membranes as a function of membrane phase state. *Biochim. Biophys. Acta.* 1768:1258–1267.
30. Callis, P. R. 1997. The theory of two-photon induced fluorescence anisotropy. *In* Topics in Fluorescence Spectroscopy: Nonlinear and Two-Photon-Induced Fluorescence, *Vol. 5*. Plenum, New York, pp. 1–42.
31. Brasselet, S., P. Ferrand, …, A. Gasecka. 2013. Imaging Molecular Order in Cell Membranes by Polarization-Resolved Fluorescence Microscopy. Berlin Heidelberg, Springer.
32. Benninger, R. K., B. Önfelt, …, P. M. French. 2005. Fluorescence imaging of two-photon linear dichroism: cholesterol depletion disrupts molecular orientation in cell membranes. *Biophys. J.* 88:609–622.
33. Opanasyuk, O., L. Ryderfors, …, L. B. Johansson. 2009. Two-photon excited fluorescence depolarization and electronic energy migration within donor-donor pairs. *Phys. Chem. Chem. Phys.* 11:7152–7160.

34. Farkas, E. R., and W. W. Webb. 2010. Multiphoton polarization imaging of steady-state molecular order in ternary lipid vesicles for the purpose of lipid phase assignment. *J. Phys. Chem. B.* 114:15512–15522.
35. Bernchou, U., J. Brewer, …, A. C. Simonsen. 2009. Texture of lipid bilayer domains. *J. Am. Chem. Soc.* 131:14130–14131.
36. Yechiel, E., and M. Edidin. 1987. Micrometer-scale domains in fibroblast plasma membranes. *J. Cell Biol.* 105:755–760.
37. Yguerabide, J., J. A. Schmidt, and E. E. Yguerabide. 1982. Lateral mobility in membranes as detected by fluorescence recovery after photobleaching. *Biophys. J.* 40:69–75.
38. Weiss, M. 2004. Challenges and artifacts in quantitative photobleaching experiments. *Traffic.* 5:662–671.
39. Wüstner, D., L. M. Solanko, …, M. A. Lomholt. 2012. Quantitative fluorescence loss in photobleaching for analysis of protein transport and aggregation. *BMC Bioinformatics.* 13:296.
40. Berkovich, R., H. Wolfenson, …, M. Urbakh. 2011. Accurate quantification of diffusion and binding kinetics of non-integral membrane proteins by FRAP. *Traffic.* 12:1648–1657.
41. Eggeling, C., C. Ringemann, …, S. W. Hell. 2009. Direct observation of the nanoscale dynamics of membrane lipids in a living cell. *Nature.* 457:1159–1162.
42. Wawrezinieck, L., H. Rigneault, …, P.-F. Lenne. 2005. Fluorescence correlation spectroscopy diffusion laws to probe the submicron cell membrane organization. *Biophys. J.* 89:4029–4042.
43. Saxton, M. J. 2007. A biological interpretation of transient anomalous subdiffusion. I. Qualitative model. *Biophys. J.* 92:1178–1191.
44. Vicidomini, G., G. Moneron, …, S. W. Hell. 2011. Sharper low-power STED nanoscopy by time gating. *Nat. Methods.* 8:571–573.
45. Kaiser, R. D., and E. London. 1998. Determination of the depth of BODIPY probes in model membranes by parallax analysis of fluorescence quenching. *Biochim. Biophys. Acta.* 1375:13–22.
46. Armendariz, K. P., H. A. Huckabay, …, R. C. Dunn. 2012. Single molecule probes of membrane structure: orientation of BODIPY probes in DPPC as a function of probe structure. *Analyst (Lond.).* 137:1402–1408.
47. Milles, S., T. Meyer, …, P. Müller. 2013. Organization of fluorescent cholesterol analogs in lipid bilayers - lessons from cyclodextrin extraction. *Biochim. Biophys. Acta.* 1828:1822–1828.
48. Taylor, M. G., T. Akiyama, …, I. C. Smith. 1982. Direct observation of the properties of cholesterol in membranes by deuterium NMR. *Chem. Phys. Lipids.* 31:359–379.
49. Przybylo, M., J. Sýkora, …, M. Hof. 2006. Lipid diffusion in giant unilamellar vesicles is more than 2 times faster than in supported phospholipid bilayers under identical conditions. *Langmuir.* 22:9096–9099.
50. Cohen, M. H., and D. Turnbull. 1959. Molecular transport in liquids and glasses. *J. Chem. Phys.* 31:1164–1169.
51. Macedo, P. B., and T. A. Litovitz. 1965. On the relative roles of free volume and activation energy in the viscosity of liquids. *J. Chem. Phys.* 42:245–256.
52. Almeida, P. F., W. L. Vaz, and T. E. Thompson. 1992. Lateral diffusion in the liquid phases of dimyristoylphosphatidylcholine/cholesterol lipid bilayers: a free volume analysis. *Biochemistry.* 31:6739–6747.
53. Gudmand, M., M. Fidorra, …, T. Heimburg. 2009. Diffusion and partitioning of fluorescent lipid probes in phospholipid monolayers. *Biophys. J.* 96:4598–4609.
54. Chung, H. S. 1966. On the Macedo-Litovitz hybrid equation for liquid viscosity. *J. Chem. Phys.* 44:1362–1364.
55. Xiang, T. 1999. Translational diffusion in lipid bilayers: dynamic free-volume theory and molecular dynamics simulations. *J. Phys. Chem. B.* 103:385–394.
56. Falck, E., M. Patra, …, I. Vattulainen. 2004. Impact of cholesterol on voids in phospholipid membranes. *J. Chem. Phys.* 121:12676–12689.
57. Lundbæck, J. A., and O. S. Andersen. 2012. Cholesterol regulation of membrane protein function by changes in bilayer physical properties - an energetic perspective. *In* Cholesterol regulation of ion channels and receptors. I. a. B. F. Levitan, editor. John Wiley & Sons, pp. 27–44.
58. O'Leary, T. J. 1987. Lateral diffusion of lipids in complex biological membranes. *Proc. Natl. Acad. Sci. USA.* 84:429–433.
59. Jensen, M. O., and O. G. Mouritsen. 2004. Lipids do influence protein function-the hydrophobic matching hypothesis revisited. *Biochim. Biophys. Acta.* 1666:205–226.
60. Niemelä, P. S., M. S. Miettinen, …, I. Vattulainen. 2010. Membrane proteins diffuse as dynamic complexes with lipids. *J. Am. Chem. Soc.* 132:7574–7575.
61. Goose, J. E., and M. S. Sansom. 2013. Reduced lateral mobility of lipids and proteins in crowded membranes. *PLOS Comput. Biol.* 9:e1003033.
62. Pomorski, T., J. C. Holthuis, …, G. van Meer. 2004. Tracking down lipid flippases and their biological functions. *J. Cell Sci.* 117:805–813.
63. Wang, T. Y., and J. R. Silvius. 2001. Cholesterol does not induce segregation of liquid-ordered domains in bilayers modeling the inner leaflet of the plasma membrane. *Biophys. J.* 81:2762–2773.
64. Leventis, R., and J. R. Silvius. 2001. Use of cyclodextrins to monitor transbilayer movement and differential lipid affinities of cholesterol. *Biophys. J.* 81:2257–2267.
65. Chiantia, S., P. Schwille, …, E. London. 2011. Asymmetric GUVs prepared by MβCD-mediated lipid exchange: an FCS study. *Biophys. J.* 100:L1–L3.
66. Hale, J. E., and F. Schroeder. 1982. Asymmetric transbilayer distribution of sterol across plasma membranes determined by fluorescence quenching of dehydroergosterol. *Eur. J. Biochem.* 122:649–661.
67. Mondal, M., B. Mesmin, …, F. R. Maxfield. 2009. Sterols are mainly in the cytoplasmic leaflet of the plasma membrane and the endocytic recycling compartment in CHO cells. *Mol. Biol. Cell.* 20:581–588.
68. Pagler, T. A., M. Wang, …, A. R. Tall. 2011. Deletion of ABCA1 and ABCG1 impairs macrophage migration because of increased Rac1 signaling. *Circ. Res.* 108:194–200.
69. Angelova, M. I., S. Soléau, …, P. Bothorel. 1992. Preparation of giant vesicles by external AC electric fields. kinetics and applications. *Prog. Colloid Polym. Sci.* 89:127–131.
70. Thévenaz, P., U. E. Ruttimann, and M. Unser. 1998. A pyramid approach to subpixel registration based on intensity. *IEEE Trans. Image Process.* 7:27–41.
71. Axelrod, D., D. E. Koppel, …, W. W. Webb. 1976. Mobility measurement by analysis of fluorescence photobleaching recovery kinetics. *Biophys. J.* 16:1055–1069.
72. Kolin, D. L., S. Costantino, and P. W. Wiseman. 2006. Sampling effects, noise, and photobleaching in temporal image correlation spectroscopy. *Biophys. J.* 90:628–639.

Membrane Orientation and Lateral Diffusion of BODIPY-Cholesterol as a Function of Probe Structure

Lukasz M. Solanko, [†] Alf Honigmann,[¶] Henrik Skov Midtiby, [‡§] Frederik W. Lund, [†] Jonathan R. Brewer, [†‡] Vjekoslav Dekaris,[‖] Robert Bittman,[‖] Christian Eggeling [¶**] and Daniel Wüstner [†*]

[†]Department of Biochemistry and Molecular Biology and [‡]MEMPHYS Center for Biomembrane Physics, Department of Pharmacy, Chemistry and Physics and [§]Institute for Chemical, Biological and Environmental Technology, University of Southern Denmark, DK-5230 Odense M, Denmark, [¶]Max Planck Institute for Biophysical Chemistry, Dept. of NanoBiophotonics, Am Fassberg 11, 37077, Göttingen, Germany, [‖]Department of Chemistry and Biochemistry, Queens College, The City University of New York, Flushing, NY 11367, USA, **Human Immunology Unit, Weatherall Institute of Molecular Medicine, University of Oxford, Oxford OX3 9DU, United Kingdom

Supporting Material

Preparation of SUVs, LUVs, and GUVs

a) SUVs and LUVs: To assess the fluorescence properties of B-P-Chol, SUVs were prepared from POPC and varying amounts of the fluorescent sterols dissolved in chloroform and ethanol, respectively. After evaporation of the solvents under a stream of nitrogen, PBS was added to the lipid film, giving a total lipid concentration of 31 μM. The lipid suspension was vortexed and afterwards sonicated using a Branson sonicator to obtain SUVs as described (1). To assess the effect of membrane curvature on fluorescence properties, we performed the same experiment with LUVs made by extrusion using a MicroExtruder (Avanti Polar Lipids, Alabaster, AL).

b) GUVs: For partition experiments, GUVs were prepared from DPPC, DOPC and cholesterol in mol percentages of 33:33:33 together with 0.5 mol% DiIC12 and 0.5 mol% of either B-Chol or B-P-Chol as described previously (1).

For polarization experiments, GUVs were prepared from 69:30 mol% POPC and cholesterol, with either 1 mol% B-Chol or B-P-Chol. Lipids were mixed in chloroform to a final total lipid concentration of 0.25 mM, from which 4 μl were deposited onto the platinum wires in the Teflon electroformation chamber. GUV electroformation was carried out over 2 h with an applied AC field with 670 V/m amplitude and 10 Hz frequency (2). For all lipid compositions, the temperature during electroformation was above the main phase transition of each phospholipid to prevent gel domain formation in the GUVs.

Preparation of supported lipid bilayers (SLBs)

SLB were prepared by spin-coating (2000 rpm) the lipid solution (2 g/l) in methanol and chloroform (1:1) on piranha-cleaned cover glass. After evaporation of the solvents under vacuum for 30 min, the membrane was hydrated with 150 mM NaCl, 10 mM Tris/HCl buffer, pH 7.5, and

rinsed with that buffer until a single clean bilayer remained. Fluorescent probes were added to the lipid solution at a final concentration of 0.01 mol%.

Fluorescence excitation and emission spectroscopy

Emission spectra of B-P-Chol in LUVs and SUVs were recorded using an ISS Chronos spectrofluorometer (ISS, Champaign, IL). The spectrofluorometer was equipped with exchangeable LED light sources for excitation, and an LED emitting light of 480 nm +/- 10 nm was used for exciting the BODIPY sterol probes. In the excitation path, a slit with 2 mm width was mounted. The emission maximum at 508 nm was plotted as a function of sterol mole fraction. The initial concentration at which B-P-Chol began to self-quench was determined, exactly as in previous measurements for B-Chol (1). Absorption spectra were recorded on a Perkin Elmer Lambda 35 spectrophotometer.

Cell culture and labelling

Fetal bovine serum (FBS) and DMEM were obtained from Gibco BRL (Life Technologies, Paisley, Scotland), if not stated otherwise. Buffer medium contained 150 mM NaCl, 5 mM KCl, 1 mM $CaCl_2$, 1 mM $MgCl_2$, 5 mM glucose, and 20 mM HEPES, pH 7.4. Baby hamster kidney (BHK) cells were grown in DMEM supplemented with 10% heat-inactivated FBS and 2 mM L-glutamine, 100 units/ml penicillin, 100 µg/ml streptomycin, 0.4 mg/ml geneticin, 0.2 µg/ml puromycin, and 1 µg/ml tetracycline. Two to three days prior to experiments, cells were seeded on microscope slide dishes coated with poly-D-lysine. Kidney epithelial cells (*Cercopithecus aethiops,* Veros) were cultured under constant conditions at 37°C and 5% CO_2 in DMEM (Invitrogen, Carlsbad, CA) containing 5% FBS (PAA, Pasching, Austria), 100 units per ml streptomycin, 100 µg/ml penicillin (all from Biochrom, Berlin, Germany), and 1 mM pyruvate (Sigma, St.Louis, MO). Fluorescent probes were stored in ethanol at a concentration of 5 mM under nitrogen at – 80°C until use. B-Chol and B-P-Chol were loaded onto methyl-β-cyclodextrin (CD) including fatty acid free bovine serum albumin (BSA) as described previously (12), giving a solution containing complexes of B-Chol/cyclodextrin (B-Chol-CD) and B-P-Chol/cyclodextrin (B-P-Chol-CD), respectively. Cells were labeled with B-Chol-CD or B-P-Chol for 1 min at 37°C, washed, and chased for 5 min, 30 min, or 60 min in buffer medium at 37°C prior to imaging.

Multicolor wide field microscopy

For co-detection of DiIC12 and BODIPY-tagged cholesterol analogs in GUVs, wide-field fluorescence microscopy and digital image acquisition were performed with a Leica DMIRBE microscope equipped with a 63x, 1.4 NA oil immersion objective (Leica Lasertechnik, Wetzlar, Germany) and an electron-multiplication Andor Ixon^{EM} blue CCD camera driven by the Solis software supplied with the camera. DiIC12 was imaged using a standard rhodamine filter set [535-nm (50-nm bandpass) excitation filter, 565-nm dichromatic mirror, and 610-nm (75-nm) bandpass) emission filter]. BODIPY-tagged cholesterol analogs were imaged using a standard fluorescein filter set [470-nm, (20-nm bandpass) excitation filter, 510-nm dichromatic mirror, and 537-nm (23-nm) bandpass) emission filter].

Two-photon excitation microscopy

Fluorescence polarization and time lapse measurements of BODIPY-tagged sterols were performed using a custom-built setup constructed around an Olympus IX70 microscope. The objective used was a 60x water immersion objective with a NA of 1.2. The excitation light source was a femtosecond Ti:Sa laser (Broadband Mai Tai XF W25 with a 10 W Millennia pump laser, 80 MHz pulse-frequency, tuneable excitation range 710-980 nm, Spectra Physics, Mountain View, CA) and the excitation wavelength used was 930 nm. For fluorescence polarization and time-lapse imaging, linear and circular polarized excitation light was used, respectively. Polarization measurements were performed by clock-wise motorized rotation of a λ half wave plate at 5^o angles giving a 10^o rotation of the incident electric field vector, ***E*** (3). One measurement consisted of acquiring 36 frames corresponding to one full rotation of the incident ***E***-vector with a count rate of 10^2 to 10^3 lasting in total for about 1 min at our set-up. For highly asymmetric dye molecules, the two-photon fluorescence emission varies as ~ $\cos^4$ to the angle between ***E*** and the electronic transition moment of the fluorophore, ***p***. For that reason, one can determine the orientation of the fluorescent group by mapping the angular intensity variation as function of the orientation of the incident electric field ***E*** (3). For a quantitative analysis, measured fluorescence must be corrected for angle variations of the emission intensity not originating from the probe response, since we found that the transmission of excitation and emission light through the optical train of the microscope depends slightly on polarization angle (3). Therefore, we performed not only measurements with both BODIPY-cholesterol probes in model and cell membranes but also with the B-Chol-CD and B-P-Chol-CD solutions. In the latter case, the fluorophore orientation is isotropic and any intensity variations are a direct measure of the instrument response. Images stacks of model and cell membranes containing the BODIPY-tagged sterols were, therefore, divided by the stacks acquired for the fluorophore solutions after adding one integer value to the latter images to avoid division by zero in all pixel positions. This also corrected for shading, i.e. spatially varying brightness differences over the image field. Afterwards, angle variations were analyzed in terms of the discrete Fourier transform of the pixel intensities as described below. To collect emission of the two BODIPY-tagged cholesterol probes, a 540 ± 25 nm filter was used (BrightLine HC). The light was detected by a photomultiplier tube (Hamamatsu H7422P-40) operated in photon-counting mode. The data were acquired using simFCS software developed by the Laboratory for Fluorescence Dynamics (University of California, Irvine, CA).

Image analysis for polarization measurements

The angle variations of fluorescence detected absorption anisotropy were analyzed by means of a discrete Fourier transform of the pixel intensities. The intensity variation of a single pixel is denoted by $I^{xy}_n(n\Delta\phi)$ where n is an integer. The complex valued discrete Fourier transform of the pixel with indices x and y is then given by:

$$\widetilde{I}^{xy}_{\gamma} = \frac{1}{N}\sum_{n=0}^{N-1} I^{xy}_{n} \cdot \exp\left(-i \cdot 2\pi \cdot \frac{\gamma \cdot n}{N}\right) \qquad \text{(S1)}$$

Here, N = 36 corresponding to the number of frames acquired every 10° for a full rotation of 360°. A $\cos^4 \phi$ intensity dependence will have a periodicity of 180° and the component $\hat{I}^{xy}_2$ will dominate with $\hat{I}^{xy}_4$ as a smaller overtone. It is sufficient to consider the principal one $\hat{I}^{xy}_2$ since the relative magnitude of these two Fourier components is constant for a $\cos^4$ dependence. The argument ½ arg($\hat{I}^{xy}_2$) depict the orientation angle of the BODIPY dipole within a given pixel. The modulus $|\hat{I}^{xy}_2|$ is a measure of the degree of orientation corresponding to the length of the molecular director **c**. The Fourier analysis using $\gamma = 2$ was performed at the single pixel level, generating a spatial map of the orientation and magnitude of the molecular director **c** (see Fig. S2D for a definition of **c**). These routines were written in MatLab (Mathworks, USA); for details, see (3). For spatial registration of image stacks, we used "StackReg" (developed by Dr. Thevenaz at the Biomedical Imaging group, EPFL, Lausanne, Switzerland) and for the image analysis we used ImageJ (developed at the U.S. National Institutes of Health and available on the Internet at http://rsb.info.nih.gov/ij) (4). Intensity profiles were measured in ImageJ and plotted in SigmaPlot 9.0 (SPSS Inc, Chicago, IL). For image visualization, ImageJ and Adobe Photoshop were used.

FRAP

FRAP experiments were performed on a Zeiss LSM510 confocal microscope. The microscope was focused on the plasma membrane on top of the cells with a pinhole size of 1 airy unit. Here a circular region of interest (ROI) with a radius, r, of 1.8 or 2.8 µm was bleached, and the fluorescence recovery was imaged over 45 frames with a laser intensity of 0.2%. This low laser power prevented significant photobleaching during image recording, as we verified in control experiments. To increase the image acquisition speed, we zoomed in on a square area with a side length of $2r$, where r is the radius of the ROI. Thus, for a ROI with radius r = 1.8 µm and r = 2.8 µm, images were acquired with a frame rate of 1.7 and 1.3 frames per sec, respectively. The fluorescence recovery curve for each image sequence was measured by determining the integrated intensity for the selected ROI (I_{ROI}) and separately for the whole cell (I_{cell}). By dividing I_{ROI} by I_{cell}, we could correct for the low photobleaching as well as for occasional small focus drifts during image recording. This is verified for the case of photobleaching in simulated FRAP experiments, as outlined below (see Fig. S7). Subsequently, the whole sequence was normalized by dividing through the prebleach intensity $F_{pre} = I_{ROI}(t=0)/I_{cell}(t=0)$, and the final recovery curve for each experiment was given by the mean of five recovery curves. To determine the lateral diffusion coefficient, one needs first the half-time of recovery (5, 6), which we determined by fitting the recovery curves to:

$$F(t) = A \cdot \left(1 - \exp(-k \cdot t)\right) + F(0) \quad \text{, with} \quad A = F(\infty) - F(0) \qquad \text{(S2a, b)}$$

Here, $F(0)$ is the fluorescence intensity at time t = 0 (i.e., immediately after bleaching), $F(\infty)$ is the final fluorescence intensity at the end of the recovery phase, and $t_{½} = \ln 2/k$ is the half time of recovery. From this the lateral diffusion constant is given by (6):

$$D = \frac{\beta r^2}{4 t_{½}}, \qquad \text{(S3)}$$

, where r is the radius of the ROI and β is a constant determined by the percentage of bleach. Here the percentage of bleach was ~55%, for which $\beta = 1.18$ (6).

FCS

FCS was performed on a home-built confocal microscope. For excitation of BODIPY, a blue laser diode (485 nm, 4μW, ≈ 80 ps pulse width, LDH-P-485B, PicoQuant) was coupled into an oil immersion objective (HCXPLAPO NA = 1.4, Leica Microsystems). Precise positioning of the laser focus in the sample and sample scanning was realized by a digital beam scanning unit (Yanus, Till-Photonics, Gräfeling, Germany) for lateral directions and a piezo scanning stage (NanoMax-TS Stage, Thorlabs, Newton, MA) for the axial direction. The fluorescence was descanned and coupled into a multi-mode fiber splitter (Fiber Optic Network Technology, Surrey, Canada) with an aperture size corresponding to 1.4× the magnified excitation spot. The fluorescence signal was then detected by single-photon counting modules (avalanche photodiode SPCM-AQR-13-FC, Perkin Elmer Optoelectronics), and the collected fluorescence counts were recorded by a single-photon counting PCI card (Becker & Hickl) or an USB correlator card (Flex02-01D, Correlator.com). Details of the FCS analysis are outlined in (7, 8). The correlation data were fitted to:

$$G(t_c) = \frac{1}{N} \cdot \left(1 + \frac{p}{(1-p)}\right) \cdot \exp\left(-\frac{t_c}{t_T}\right) \cdot \frac{1}{1 + \left(\frac{t_c}{\tau_D}\right)^{\alpha}} \qquad \text{(S4)}$$

, where N is the particle number (i.e., the mean number of fluorescent molecules in the detection volume), which is proportional to the concentration divided by the measurement volume (or area for two-dimensional samples), p is the fraction of dye that is on average in the dark triplet state, t_T is the triplet correlation time, τ_D is the average transit time of the fluorescent molecules diffusing through the observation area, and α is the anomaly exponent, which is 1 if the diffusion is free and <1 for anomalous hindered diffusion. All FCS measurements were performed at the lower, surface attached part of the PM.

STED-FCS

Sub-diffraction observation spots were obtained using STED-microscopy (22). BODIPY fluorescence was depleted with a 577 nm continuous-wave optically pumped semiconductor laser (Coherent). The doughnut-shaped focal intensity distributions of the STED beam featuring a central zero was produced by introducing a phase-modifying plate (RPC Photonics) into the beam path, imprinting a helical phase ramp ($\exp(i\varphi)$ with $0 \leq \varphi \leq 2\pi$) onto the wave front. A λ/4-plate ensured circular polarization of the STED and of the excitation beam. The maximum laser power in the objective was ~80 mW for the 577 nm STED and 4 μW for the 485nm excitation laser. The effective resolution was further enhanced by time gating the photon arrival times of the detected fluorescence using a software routine in MATLAB (9). All STED-FCS measurements were performed at the lower, surface attached part of the PM.

Derivation of Eq. 2 of the main text

We will start from Eq. 1 of the main text with only one angular dependence of the fluorescence response for polarized two-photon excitation (i.e. $\theta_0^2=0$, $\theta_0^1=\theta_0$, $A_1=A$) neglecting the background term, F_0. Orientation fluctuation of θ_0 can be modeled by an additive normal distributed component, ε, with zero mean value giving:

$$E\{F(\theta)\}=E\left\{A\cdot\cos(\theta-\theta_0-\varepsilon)^4\right\}=E\left\{A\cdot\left(\frac{3}{8}+\frac{1}{2}\cdot\cos(2\cdot(\theta-\theta_0-\varepsilon))+\frac{1}{8}\cdot\cos(4\cdot(\theta-\theta_0-\varepsilon)\right)\right\} \quad \text{(S5)}$$

Using the relation $\cos(x-y)=\cos(x)\cdot\cos(y)-\sin(x)\cdot\sin(y)$, the right hand side of Eq. S5 can be expanded as Eq. S(6):

$$E\left\{A\cdot\left(\frac{3}{8}+\frac{1}{2}\cdot\cos(2\theta-2\theta)\cdot\cos(2\varepsilon)-\frac{1}{2}\cdot\sin(2\theta-2\theta)\cdot\sin(2\varepsilon)+\frac{1}{8}\cdot\cos(4\theta-4\theta)\cdot\cos(4\varepsilon)-\frac{1}{8}\cdot\sin(4\theta-4\theta)\cdot\sin(4\varepsilon)\right)\right\}$$

The expectation value of a function, $f(\varepsilon)$, is the first moment of the probability density function (PDF), $p(\varepsilon)$, and can be written as:

$$E\{f(\varepsilon)\}=\int_{-\infty}^{+\infty}f(\varepsilon)\cdot p(\varepsilon)d\varepsilon \quad \text{(S7)}$$

The expectation value of the sine function for a Gaussian PDF with zero mean and standard deviation σ is:

$$E\{\sin(\varepsilon)\}=\int_{-\infty}^{+\infty}\sin(\varepsilon)\cdot\frac{1}{\sigma\sqrt{2\pi}}\cdot\exp\left(\frac{-\varepsilon^2}{2\sigma^2}\right)d\varepsilon=0 \quad \text{(S8)}$$

As the integral of an odd function over a symmetric interval is zero, the expectation value of $\sin(\varepsilon)$ is zero as well. Since the cosine function is even, its expectation value is not zero but can be expressed by a Taylor expansion according to

$$E\{\cos(\varepsilon)\}=\int_{-\infty}^{+\infty}\sum_{m=0}^{\infty}\frac{(-1)^m\cdot\varepsilon^{2m}}{(2m)!}\cdot\exp\left(\frac{-\varepsilon^2}{2\sigma^2}\right)d\varepsilon=\sum_{m=0}^{\infty}\frac{(-1)^m}{(2m)!}\int_{-\infty}^{+\infty}\varepsilon^{2m}\cdot\exp\left(\frac{-\varepsilon^2}{2\sigma^2}\right)d\varepsilon \quad \text{(S9)}$$

The integrand on the right hand side comprises the even central moments of the normal distribution which have the values:

$$\int_{-\infty}^{+\infty} \varepsilon^{2m} \cdot \exp\left(\frac{-\varepsilon^2}{2\sigma^2}\right) d\varepsilon = \frac{(2m)!}{2^m \cdot m!} \cdot \sigma^{2m} \tag{S10}$$

Using Eq. S10 in S9 we get:

$$E\{\cos(\varepsilon)\} = \sum_{m=0}^{\infty} \frac{(-1)^m}{(2m)!} \cdot \frac{(2m)!}{2^m \cdot m!} \cdot \sigma^{2m} = \sum_{m=0}^{\infty} \frac{1}{m!} \cdot \left(\frac{-\sigma^2}{2}\right)^m = \exp(-\sigma^2 / m) \tag{S11}$$

Use of Eqs. S8 and S11 in Eq. S6 gives Eq. 2 of the main text.

Simulation of FRAP experiment in the presence of photobleaching during image recording

To illustrate the effect of photobleaching during the recovery process, we set up a FRAP reaction-diffusion simulation in MatLab. Here 150,000 particles were moving by Brownian diffusion with a diffusion constant of D = 0.1 μm^2/sec in a square area with a side length of 5 μm and periodic boundaries. Initially, 5 steps of diffusion were simulated in the equilibrated system to determine the number of fluorophores in the ROI pre-bleach. Then all fluorophores in the ROI with radius 1 μm were bleached and the recovery was monitored over 94 additional iterations of Brownian diffusion. During the simulated recovery phase, fluorophores could slowly bleach in the whole field with a given rate constant. For each iteration the number of fluorophores to bleach was calculated as described by Kolin *et al.* (10):

$$N_n^{bleach} = poissrnd\left(N_{n-1} - N_{n-1} \exp\left[-k\Delta t\right]\right), \tag{S12}$$

where n is the number of the current frame, $N_{n\text{-}1}$ is the number of fluorescent particles in frame n-1, k is the rate constant for bleaching, Δt is the time between two subsequent images and *poissrnd* is an inherent MatLab function which generates a random number from a Poisson distribution with a given mean. The effect of photobleaching during recovery is shown in Fig. S7A, while Fig. S7B shows the total number of fluorescent particles in the simulated area – including the ROI - as a function of time. From this it can be seen that for moderate bleaching during recovery (green curve, k = 0.001 s^{-1}) the percentage of bleach is reduced while the recovery curve still looks as expected

for a FRAP experiment. This resembles the situation we faced with the two BODIPY-cholesterol's. For stronger bleaching the recovery curve starts to decay after an initial period of recovery (blue and red curves, $k = 0.005\ s^{-1}$ and $k = 0.01\ s^{-1}$, respectively). Bleaching during recovery is corrected for by dividing the measured fluorescence recovery curve by the total fluorescence intensity of the imaged area. This is illustrated in Fig. S7C, where the number of fluorophores in the ROI was divided by the total number of fluorophores. This method provided the correct amplitude and half-time of recovery and thereby identical diffusion constants in the simulation.

Synthesis of B-P-Chol

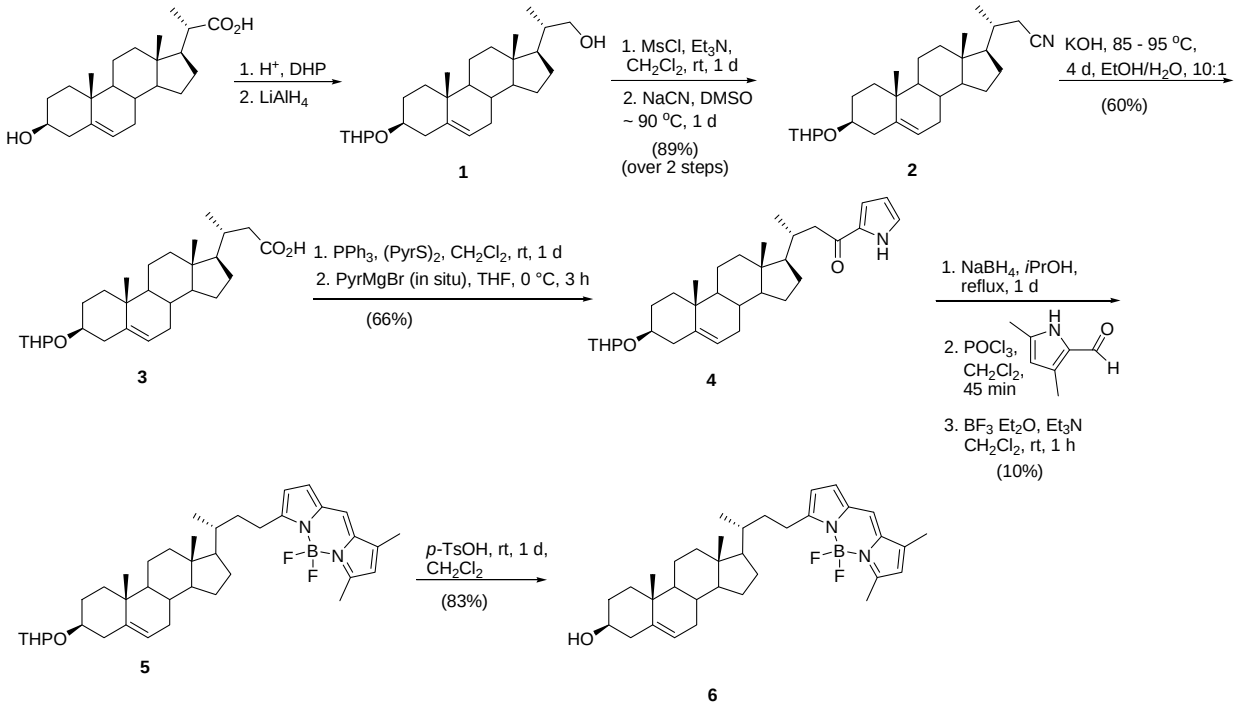

Syntheses of the intermediates and the target probe, B-P-Chol

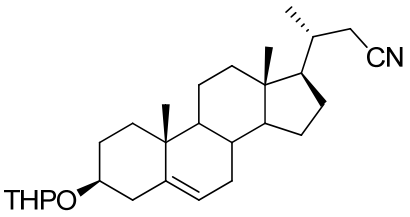

2

Cholesterol derivative **1** (1.40 g, 3.36 mmol) was dissolved in CH_2Cl_2 (30 mL) and subsequently MsCl (1.26 mL, 16.2 mmol) and Et_3N (4.77 mL, 34.2 mmol) were added. The reaction mixture was stirred at rt for 1 d. The solution was washed with H_2O (3 x 20 mL), dried with $MgSO_4$, filtered, and concentrated in vacuo, affording 1.81 g of the crude mesylated cholesterol derivative. No purification was performed. After the crude mesylated cholesterol derivative (1.81 g) was dissolved in DMSO (20 mL), NaCN (360 mg, 7.31 mmol) was added. The reaction mixture was heated to 90 °C and stirred for 1 d. After the mixture was cooled to rt, H_2O (20 mL) was added. The mixture was extracted with Et_2O (3 x 20 mL) and washed with water (30 mL) and brine (30 mL). The crude product was purified by silica gel chromatography (hexane, hexane/EtOAc gradient: 4:1, 2:1, 1:1), providing 990 mg (89%) of compound **2** as a colorless amorphous solid; mp 170 °C; $[\alpha]_D^{25}$ -36.4 (*c* 0.62, $CHCl_3$); ^{1}H NMR (400 MHz, $CDCl_3$): δ 0.70 (s, 3H), 0.89 - 1.31(m, 14H), 1.38 - 2.01 (m, 21H), 2.15 - 2.39 (m, 4H), 3.44 - 3.58 (m, 2H), 3.88 - 3.95 (m, 1H), 4.69 - 4.74 (m, 1H), 5.31 - 5.37 (m, 1H); ^{13}C NMR (101 MHz, $CDCl_3$): δ 12.1, 19.48, 19.51, 19.8, 20.2, 20.3, 21.07, 21.09, 24.3, 25.0, 25.6, 28.1, 28.2, 29.8, 31.1, 31.42, 31.44, 31.94, 31.96, 32.0, 33.7, 36.87, 36.91, 37.3, 37.6, 38.9, 39.5, 40.4, 42.6, 50.08, 50.11, 54.9, 56.6, 63.0, 63.1, 76.08, 76.11, 97.0, 97.2, 119.2, 121.4, 141.0, 141.2. ESI-HRMS: $C_{28}H_{43}NO_2$ calcd. 448.3186 $[M+Na]^+$, found 448.3181.

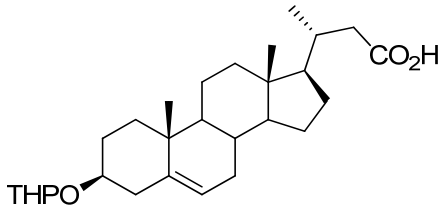

3

Cholesterol nitrile derivative **2** (975 mg, 2.29 mmol) was suspended in EtOH (15 mL). Then a solution of KOH (2.57 g, 45.8 mmol) in H_2O (1.5 mL) was added, and the mixture was heated at reflux for 4 d. After the mixture was cooled to rt, the solvents were evaporated and H_2O (5 mL) was added to the residue. The mixture was extracted with Et_2O (2 x 5 mL). Then the pH was set to 5 - 6 by careful addition of HCl (3 N), and the mixture extracted with CH_2Cl_2 (3 x 5 mL). The combined CH_2Cl_2 layers were dried with $MgSO_4$. Filtration and removal of the solvent in vacuo afforded crude **3** as a yellow oil. The crude product was purified by silica gel chromatography (hexane/EtOAc gradient: 2:1, 1:1, 1:2; EtOAc), giving 611 mg (60%) of compound **3** as an amorphous solid; mp 195 °C; $[\alpha]_D^{25}$ -35.2 (*c* 1.2, $CHCl_3$); ^{1}H NMR (400 MHz, $CDCl_3$): δ 0.71 (s, 3H), 0.85 - 1.35 (m, 14H), 1.38 - 2.06 (m, 20H), 2.14 - 2.38 (m, 2H), 2.47 (dd, *J* = 5.5, 6.2 Hz, 1H), 3.43 - 3.58 (m, 2H), 3.86 - 3.97 (m, 1H), 4.66 - 4.78 (m, 1H), 5.30 - 5.37 (m, 1H); ^{13}C NMR (101 MHz, $CDCl_3$): δ 12.0, 19.5, 19.7, 20.1, 20.2, 21.12, 21.14, 24.3, 25.6, 28.1, 28.4, 31.40, 31.36, 32.0, 33.8, 36.87, 36.91, 37.3, 37.6, 38.9, 39.7, 40.3, 41.4, 42.6, 50.17, 50.21, 55.9, 56.9, 62.9, 63.0, 76.1,

96.9, 97.1, 121.5, 121.6, 141.0, 141.2, 179.6; ESI-HRMS: $C_{28}H_{44}O_4$ calcd. 467.3132 $[M+Na]^+$, found 467.3132.

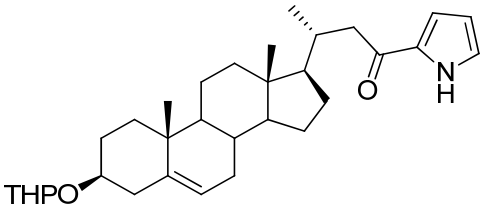

4

PPh_3 (1.69 mmol) and 1,1`-dipyridyl disulfide ($(PyrS)_2$), 1.69 mmol) were dissolved in CH_2Cl_2 (6 mL) and stirred for 15 min. Then a solution of bisnorcholenic acid derivative **3** (577 mg, 1.30 mmol) in CH_2Cl_2 (12 mL) was added, and the reaction mixture was stirred overnight. The solvent was evaporated and the residue was dissolved in THF (10 mL). A solution of MeMgBr (3.71 mL, 5.20 mmol; 1.4 M in toluene/THF) was mixed with THF (5 mL) and cooled to 0 °C. Then pyrrole (469 uL, 6.76 mmol) was added dropwise, and the reaction mixture was stirred for 40 min at 0 °C. A 10-mL solution of the activated ester was added dropwise and the mixture was stirred for an additional 3 h at 0 °C. The solvents were evaporated, the residue was dissolved in CH_2Cl_2 (50 mL), and the solution was cooled to 0 °C and quenched with aqueous saturated NH_4Cl solution (15 mL). The organic layer was separated and the aqueous layer was extracted with CH_2Cl_2 (3 x 15 mL). The combined organic layers were washed with 5% aqueous K_2CO_3 solution (50 mL), H_2O (50 mL), and brine (50 mL), and then dried with $MgSO_4$. Filtration and evaporation of the solvent gave crude pyrrole derivative **4**. Purification by silica gel chromatography (hexane/EtOAc gradient: hexane; 40:1, 20:1, 12:1, 8:1, 4:1) afforded 421 mg (66%) of ketone **4** as a colorless amorphous solid; mp 181 °C $[\alpha]_D^{25}$ -34.4 (*c* 0.47, $CHCl_3$); ^{1}H NMR (500 MHz, $CDCl_3$): δ 0.73 (s, 3H), 0.82 - 1.29 (m, 14H), 1.32 - 1.76 (m, 12H), 1.78 - 2.05 (m, 6H), 2.06 - 2.39 (m, 3H), 2.43 - 2.54 (m, 1H), 2.74 - 2.83 (d, J = 14.3 Hz, 1H), 3.43 - 3.58 (m, 2H), 3.87 - 3.96 (m, 1H), 4.71 (s, 1H), 5.34 (m, 1H), 6.26 (s, 1H), 6.89 (s, 1H), 7.01 (s, 1H) 9.68 (s, 1H); ^{13}C NMR (100 MHz, $CDCl_3$): δ 12.0, 19.5, 19.8, 20.1, 20.2, 21.1, 24.4, 25.6, 28.1, 28.7, 29.8, 31.4, 32.0, 34.3, 36.8, 36.9, 37.3, 37.5, 38.9, 39.8, 40.3, 42.7, 45.2, 50.19, 50.23, 56.7, 56.9, 62.9, 63.0, 76.1, 97.0, 97.1, 110.6, 116.3, 121.5, 121.6, 124.6, 133.0, 141.0, 141.2, 191.4; ESI-HRMS: $C_{32}H_{47}NO_3$ calcd. 494.3629 $[M+Na]^+$, found 494.3626.

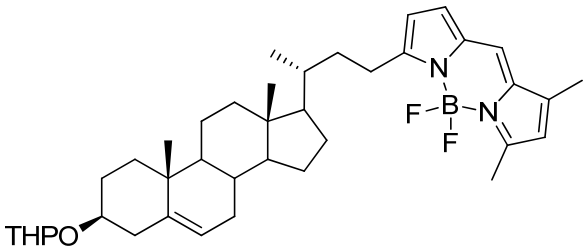

5

To a solution of ketone **4** (10 mg, 0.023 mmol) in *i*-PrOH (1.5 mL) was added $NaBH_4$ (4.5 mg, 0.12 mmol). The reaction mixture was heated at reflux for 1 d. After the mixture was cooled to rt, H_2O (1.5 mL) was added, and the mixture was extracted with CH_2Cl_2. The combined organic layers were washed with H_2O (2 mL) and brine (2 mL). After the organic layer was dried with $MgSO_4$ and filtered, the solvent was removed in vacuo, providing 12 mg of compound **5** as a colorless oil. No purification was performed. The crude product was dissolved in CH_2Cl_2 (2 mL) and 3,5-

dimethylpyrrole carboxaldehyde (25.5 mg, 0.210 mmol) and $POCl_3$ (2.05 μL, 0.021 mmol) were added. The reaction mixture was stirred for 45 min at rt. Then Et_3N (41.0 mL, 0.294 mmol) and $BF_3{\cdot}OEt_2$ (42.5 mL, 0.336 mmol) were added and stirring was continued for 1 h at rt. The solution was washed with H_2O (3 x 1 mL) and dried with $MgSO_4$. After filtration and evaporation, crude BODIPY derivative **5** was isolated as a dark blue oil. The crude product was purified by silica gel chromatography (hexane/EtOAc gradient: hexane; 40:1, 20:1, 12:1, 8:1, 4:1) followed by preparative TLC (hexane/EtOAc 8:1) to afford 1.4 mg (10%) of BODIPY derivative **5** as a red amorphous solid together with some of target compound **6** (which presumably formed when the THP was removed during the NMR spectroscopy of **5** in $CDCl_3$). ^{1}H NMR (500 MHz, $CDCl_3$): δ 0.73 (s, 3H), 0.79 - 1.73 (m, 14H), 1.81 - 1.92 (m, 2H), 1.98 - 2.05 (m, 2H), 2.32 - 2.38 (m, 2H), 2.44 - 2.52 (m, 1H), 2.76 - 2.81 (m, 1H), 3.44 - 3.55 (m, 2H), 3.88 - 3.96 (m, 1H), 4.70 - 4.73 (m, 1H), 5.32 - 5.37 (m, 1H), 6.25 - 6.29 (m, 1H), 6.87 - 6.90 (m, 1H), 6.99 - 7.02 (m, 1H); ESI-HRMS: $C_{39}H_{55}BF_2N_2O_2$ calcd. 633.4397 $[M+H]^+$, found 633.4401. $C_{34}H_{47}BF_2N_2O_2$ calcd. 549.3822 $[M+H]^+$, found 549.3831.

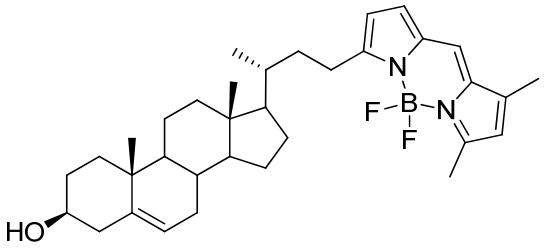

6

BODIPY derivative **5** (1.4 mg, 2.2 μmol) was dissolved in CH_2Cl_2 (0.4 mL) and *p*-TsOH (0.4 mg, 2.2 μmol) was added. The mixture was stirred for 1 d at rt. The solvent was evaporated and the crude product was purified by preparative TLC (hexane/EtOAc 4:1), affording 1 mg (83%) of B-P-Chol (**6**) as a red amorphous solid. ^{1}H NMR (400 MHz, $CDCl_3$): δ 0.67 (s, 3H), 0.76 - 1.69 (m, 14H), 1.78 - 2.03 (m, 11H), 2.22 (s, 3H), 2.23 - 2.30 (m, 2H), 2.31 - 2.35 (m, 1H), 2.54 (s, 3H), 2.95 - 3.02 (m, 1H), 3.47 - 3.54 (m, 1H), 3.60 - 3.64 (m, 1H), 5.34 (m, 1H), 6.06 (s, 1H), 6.25 (d, J = 4.15 Hz, 1H), 6.88 (d, J = 3.85 Hz, 1H), 7.03 - 7.04 (m, 1H); ESI-HRMS: $C_{34}H_{47}BF_2N_2O_2$ calcd. 549.3822 $[M+H]^+$, found 549.3829.

Supporting figures

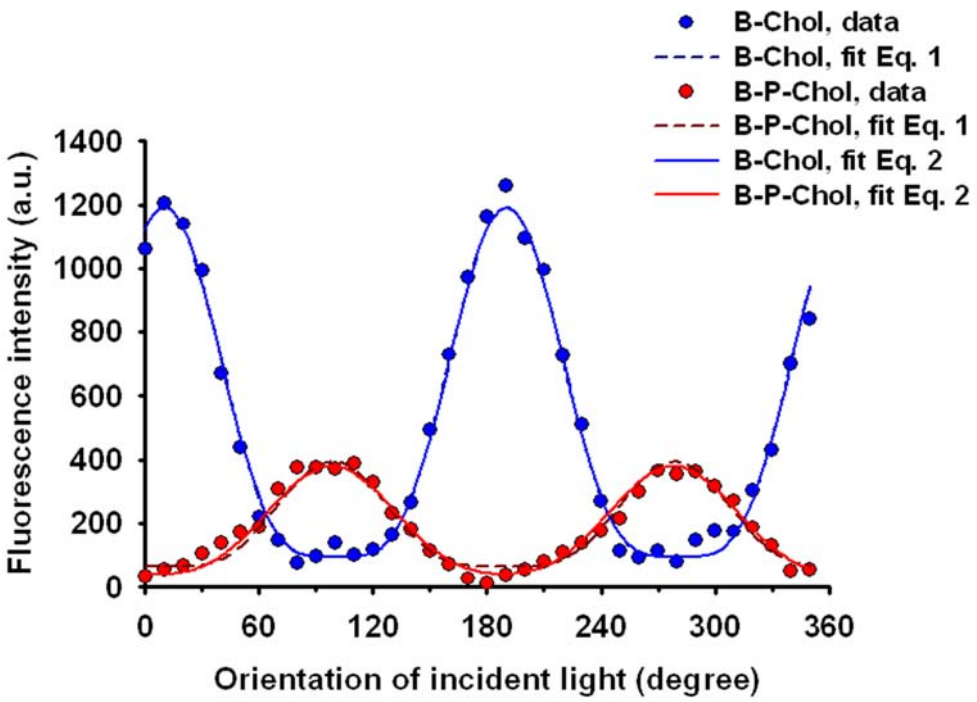

Fig. S1. Non-linear fit of Eqs. 1 and 2 to polarimetry data of BODIPY-cholesterol probes in GUVs. Fluorescence response of B-Chol (blue symbols; data, blue lines, fits) and B-P-Chol (red symbols; data, red lines, fits) in GUVs prepared from POPC and cholesterol (7:3 molar ratio) as a function of the rotation angle of the incident linearly polarized excitation light (compare Fig. 2 in the main text). Fit to Eq. 1 (dashed lines) and Eq. 2 of the main text (straight lines) gave almost indistinguishable results.

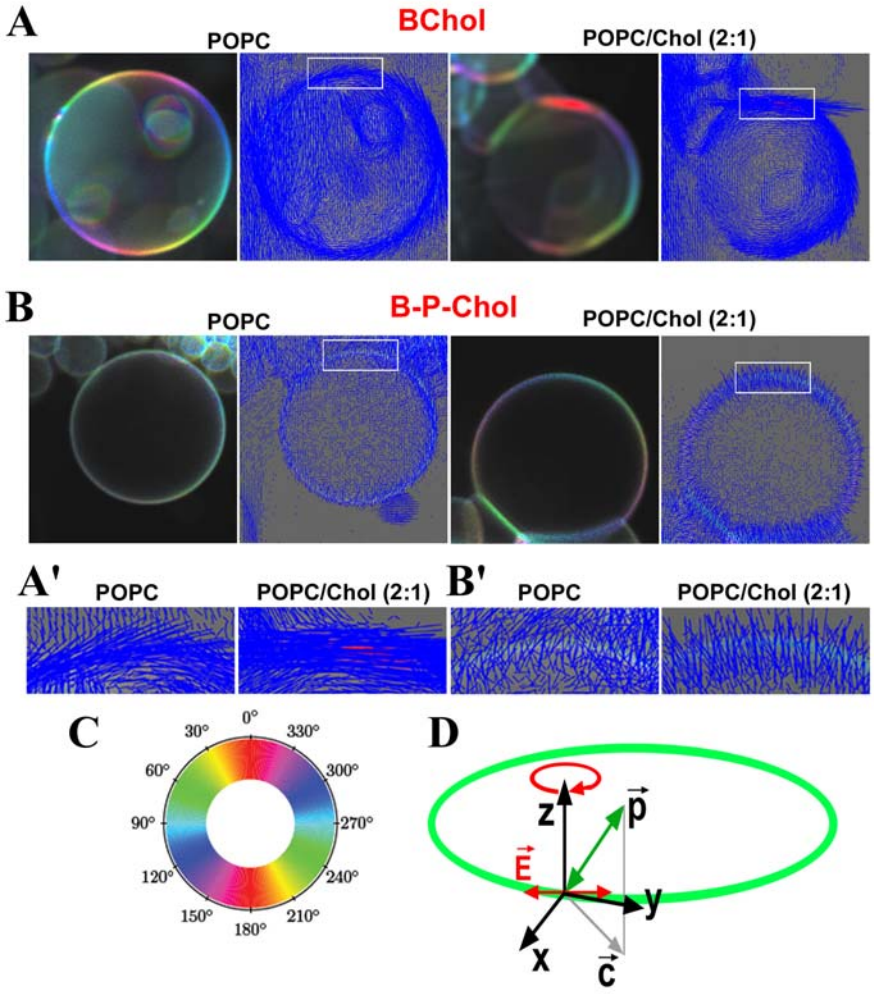

Fig. S2. Pixel-based Fourier analysis of two-photon polarimetry data in model membranes. The fluorescence response of B-Chol (A) and B-P-Chol (B) to the rotating incident field vector, ***E***, was analyzed using a discrete Fourier transform of the pixel intensities. The two left images in panels A and B show the color- and vector-coded representation of the fluorescence response, respectively, for B-Chol and B-P-Chol in GUVs made of POPC only. The two right images of panel A and B show the same analysis for both sterol probes in GUVs made of POPC and cholesterol. The rectangular box highlights a region used for zoom of the vector-coded representation in panels A' and B'. Clearly, the small blue lines are oriented almost parallel to the GUV bilayer for B-Chol (A'), while they align perpendicular to the GUV membranes in the case of B-P-Chol (B'). C, color palette used for color-coding of the angle of fluorescence response relative to the incident field in the HSV color model. D, basis of the vector-coded representation: in the laboratory coordinate system with unit vectors *x*, *y*, *z*, the linearly polarized excitation light vector, ***E***, is given in red, making a full rotation in 10^{o} steps yielding 36 images per recording. The main excitation transition moment of the fluorophores is shown as the vector ***p*** in green. The equatorial plane of the GUV appears as a circle shown in green in the microscope focal plane, while the vector ***p*** can have non-vanishing components out of this plane. Detected is the projection of the transition moment vector ***p*** into the focal plane given by the director ***c*** (grey arrow in panel D).

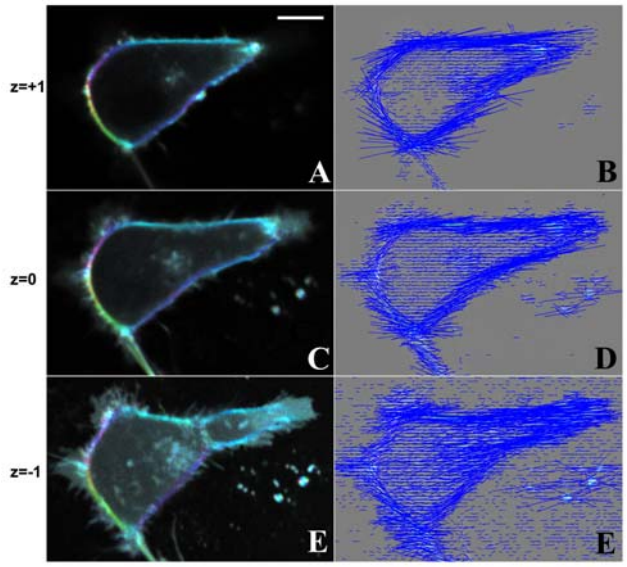

Fig. S3. Two-photon polarimetry of B-Chol in BHK cells at various axial positions. BHK cells were labeled with B-Chol/CD for 1 min, washed with the buffer medium, and imaged on a two-photon microscope with 10° rotation of the incident linearly polarized electric field vector, ***E***. Between recordings of a full rotation consisting of 36 images the focal position was shifted by 1.0 µm downwards in the axial direction starting with a position on the upper half of the cell (A, B; 'z=1') to the cell equator (C, D; 'z=0') and finally to the cell-substrate contact side (E, F; 'z=-1'). The color-coded (A, C, E) and vector-coded (B, D, F) presentation of the fluorescence response is shown. Scale bar = 10 µm.

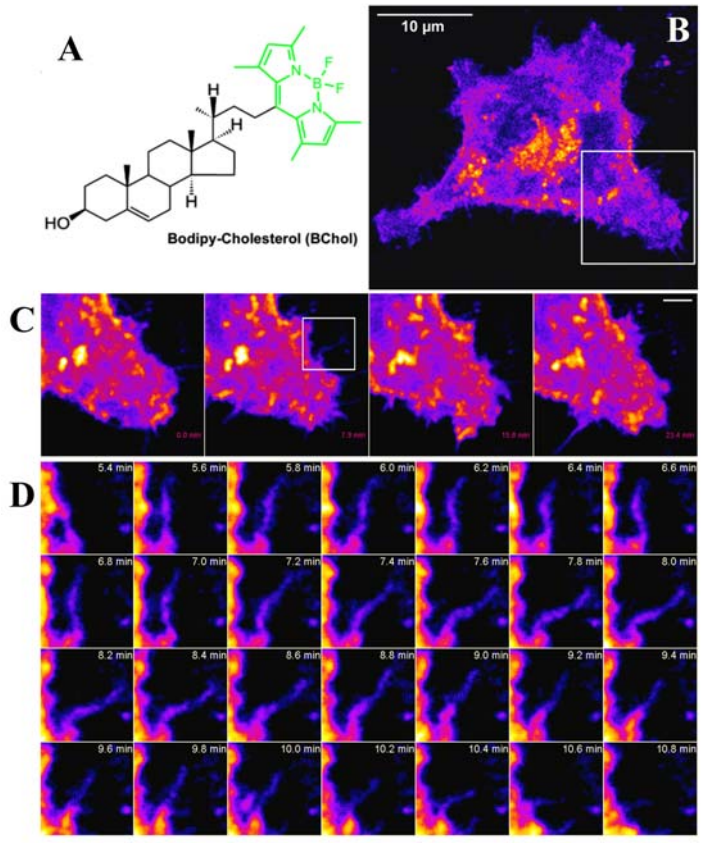

Fig. S4. Two-photon time-lapse imaging of membrane ruffling dynamics in BHK cells. BHK cells were labeled with B-Chol/CD for 1 min, washed with the buffer medium, and imaged on a two-photon microscope for more than 10 min with a frame rate of 0.1 Hz. **A**, B-Chol with the structure of the fluorophore shown in green. B, view of the imaged cell with zoomed box being enlarged in panel C. D, dynamics of the region indicated in the zoom box of panel C. Membrane ruffling and dynamically changing surface protrusions are visible, especially at cell attachment regions. Scale bar in panel C = 1.5 µm.

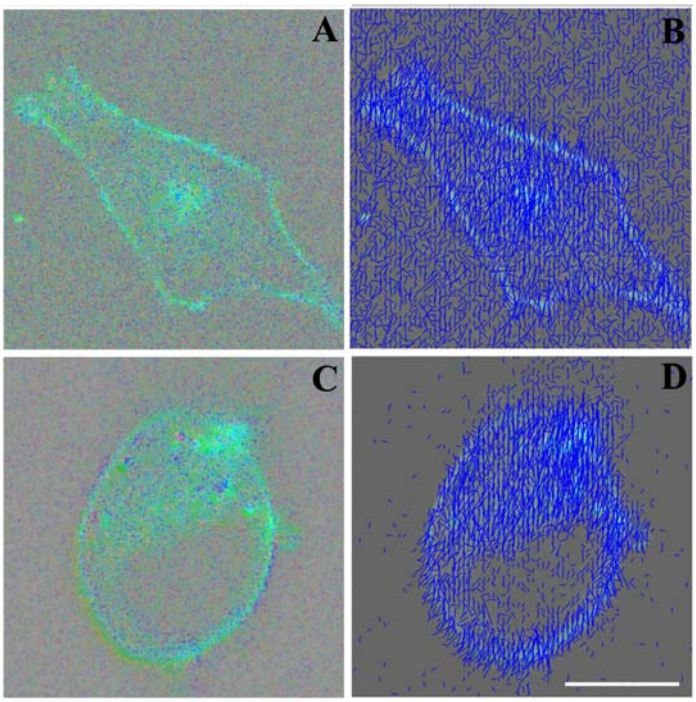

Fig. S5. Two-photon fluorescence polarimetry of B-P-Chol in cell membranes. BHK cells were labeled with B-P-Chol from a B-P-Chol-CD complex as described above. Cells were imaged on a two-photon microscope with 10^{o} rotation of the incident linearly polarized electric field vector, ***E***. The start position of ***E*** is horizontal, as indicated in the legend to Fig. 2B. A, B, show the color-coded (A) and vector-coded (B) presentation of the fluorescence response for intact cells. For C and D, cells were treated with 20 μM cytochalasin for 30 min to disrupt actin. The color-coded (C) and vector-coded (D) presentation of the fluorescence response is shown for a representative cytochalasin-treated cell labeled with B-P-Chol. Scale bar = 15 μm.

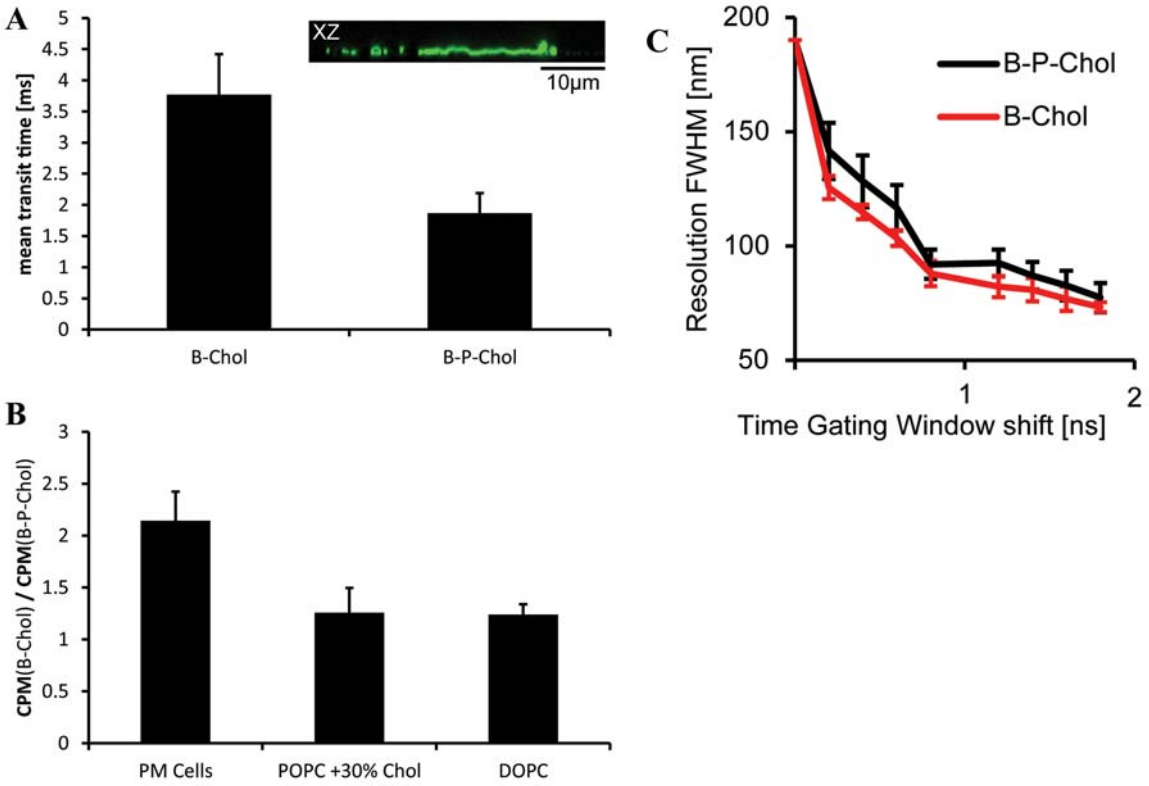

Fig. S6. STED-FCS control experiments

A, Confocal FCS data of B-Chol and B-P-Chol in PM sheets of live Vero cells revealing similar average transit times as measurements in intact Vero cells. Inset: Scanning xz fluorescence image of B-P-Chol in the membrane sheets. B, Ratio of the single-molecule fluorescence brightness (CPM: counts-per-particle) of B-Chol and B-P-Chol in the PM of living Vero cells (PM cells) and in supported lipid bilayers (DOPC: one-component DOPC; POPC + 30% Chol: two-component system POPC and 30 mol% cholesterol) as determined by FCS, demonstrating a 2-fold difference in brightness only for the PM, which is in agreement with the difference in diffusion coefficients. C, Calibration of the STED-FCS measurements: the spatial resolution or full-width-at-half-maximum (FWHM) of the observation spot as determined from the average transit times of the FCS measurements of B-Chol and B-P-Chol in DOPC supported lipid bilayers at 80 mW STED power for different positions of the gated detection (time gating window shift) (44).

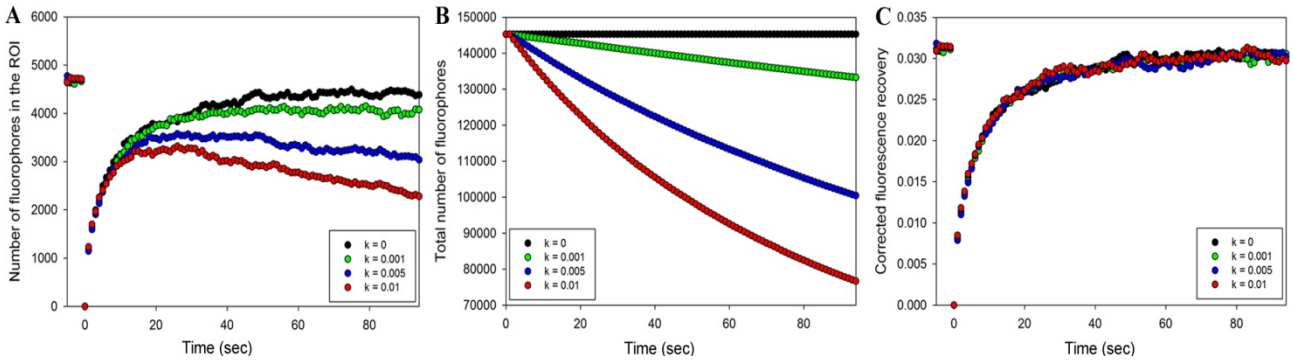

Fig. S7. Normalization of simulated FRAP data to correct for photobleaching during acquisition. A, FRAP curves for simulated experiments with different bleach rates during fluorescence recovery. B, curves of the total number of fluorophores as a function of time for the same bleach rates. C, recovery curves were corrected by dividing the measured recovery curve (A) by the total number of fluorophores (B).

SUPPORTING REFERENCES

1. Wüstner, D., L. M. Solanko, E. Sokol, F. W. Lund, O. Garvik, Z. Li, R. Bittman, T. Korte, and A. Herrmann. 2011. Quantitative Assessment of Sterol Traffic in Living Cells by Dual Labeling with Dehydroergosterol and BODIPY-cholesterol. Chem. Phys. Lipids 164:221-235.
2. Angelova, M. I., S. Soléau, P. Méléard, J. F. Fuaucon, and P. Bothorel. 1992. Preparation of giant vesicles by external AC electric fields. kinetics and applications. Prog. Colloid Polym. Sci. 89:127-131.
3. Bernchou, U., J. Brewer, H. S. Midtiby, J. H. Ipsen, L. A. Bagatolli, and A. C. Simonsen. 2009. Texture of lipid bilayer domains. J. Am. Chem. Soc. 131:14130-14131.
4. Thevenaz, P., U. E. Ruttimann, and E. Unser. 1998. A pyramid approach to subpixel registration based on intensity. IEEE Transactions on Image Processing 7:27-41.
5. Axelrod, D., Koppel, D.E., Schlessinger, J., Elson, E., and Webb, W.W. 1976. Mobility measurement by analysis of fluorescence photobleaching recovery kinetics. Biophys. J. 16:1055-1069.
6. Yguerabide, J., J. A. Schmidt, and E. E. Yguerabide. 1982. Lateral mobility in membranes as detected by fluorescence recovery after photobleaching. Biophys. J. 40:69-75.
7. Mueller, V., C. Ringemann, A. Honigmann, G. Schwarzmann, R. Medda, M. Leutenegger, S. Polyakova, V. N. Belov, S. W. Hell, and C. Eggeling. 2011. STED nanoscopy reveals molecular details of cholesterol- and cytoskeleton-modulated lipid interactions in living cells. Biophys. J. 101:1651-1660.
8. Klar, T. A., S. Jakobs, M. Dyba, A. Egner, and S. W. Hell. 2000. Fluorescence microscopy with diffraction resolution barrier broken by stimulated emission. Proc. Nat. Acad. Sci. U. S. A. 97:8206-8210.
9. Vicidomini, G., G. Moneron, K. Y. Han, V. Westphal, H. Ta, M. Reuss, J. Engelhardt, C. Eggeling, and S. W. Hell. 2011. Sharper low-power STED nanoscopy by time gating. Nat. Methods 8:571-573.
10. Kolin, D. L., S. Costantino, and P. W. Wiseman. 2006. Sampling Effects, Noise, and Photobleaching in Temporal Image Correlation Spectroscopy. Biophysical Journal 90:628-639.